AD_____

Award Number: DAMD17-03-1-0576

TITLE: Assessment of the Genetic Variation in Bone Fracture Healing

PRINCIPAL INVESTIGATOR: Louis C. Gerstenfeld, Ph.D.

CONTRACTING ORGANIZATION: Trustees of Boston University
Boston, MA 02118-2394

REPORT DATE: January 2006

TYPE OF REPORT: Final

PREPARED FOR: U.S. Army Medical Research and Materiel Command
Fort Detrick, Maryland 21702-5012

REPORT DOCUMENTATION PAGE

Form Approved
OMB No. 0704-0188

1. REPORT DATE *(DD-MM-YYYY)*	2. REPORT TYPE	3. DATES COVERED *(From - To)*
01-01-2006	Final	1 Apr 03 – 31 Mar 2005

4. TITLE AND SUBTITLE
Assessment of the Genetic Variation in Bone Fracture Healing

5a. CONTRACT NUMBER

5b. GRANT NUMBER
DAMD17-03-1-0576

5c. PROGRAM ELEMENT NUMBER

6. AUTHOR(S)
Louis C. Gerstenfeld, Ph.D.

E-Mail: lgersten@bu.edu

5d. PROJECT NUMBER

5e. TASK NUMBER

5f. WORK UNIT NUMBER

7. PERFORMING ORGANIZATION NAME(S) AND ADDRESS(ES)

Trustees of Boston University
Boston, MA 02118-2394

8. PERFORMING ORGANIZATION REPORT NUMBER

9. SPONSORING / MONITORING AGENCY NAME(S) AND ADDRESS(ES)
U.S. Army Medical Research and Materiel Command
Fort Detrick, Maryland 21702-5012

10. SPONSOR/MONITOR'S ACRONYM(S)

11. SPONSOR/MONITOR'S REPORT NUMBER(S)

12. DISTRIBUTION / AVAILABILITY STATEMENT
Approved for Public Release; Distribution Unlimited

13. SUPPLEMENTARY NOTES

14. Abstract

The hypothesis of these studies is that genetic processes that lead to the variations in both structural and material properties of bone development will be recapitulated in the developmental mechanism(s) that controls the bone quality during fracture healing. Two goals were set out in this proposal to test this hypothesis. The first was to determine how variations in basic bone quality in the three in bred strains of mice were expressed during fracture healing. MicroCT and mechanical testing of day 21 and 35 fracture calluses demonstrated that each strain recapitulated their variations in geometric and material (BMD/BMC) properties during fracture healing. Furthermore, variations in bone quality differentially effected the rates of healing (i.e. there are genetic variations slow versus fast bone healing). The second goal was directed at identifying the underlying biological processes that lead to genetic variation, which effect both bone quality and rates of fracture healing. Our data demonstrate that there is genetic variation in rates endochondral bone formation during fracture healing which recapitulate differences seen in original bone growth (i.e. genetic strains that show slow or fast epiphyseal growth show slow or fast fracture healing. Large scale transcriptional profiling initiated during the tenure of this grant is ongoing to further define genetic variability in fracture healing.

15. SUBJECT TERMS
BMD, Genetics Determinants, Fracture Healing, Biomechanics, Genomic Expression Profiling

16. SECURITY CLASSIFICATION OF:			17. LIMITATION OF ABSTRACT	18. NUMBER OF PAGES	19a. NAME OF RESPONSIBLE PERSON
a. REPORT	b. ABSTRACT	c. THIS PAGE			USAMRMC
U	U	U	UU	84	19b. TELEPHONE NUMBER *(include area code)*

Table of Contents

INTRODUCTION

Studies have shown that individuals with a small moment of inertia (slender bones) are at higher risk of developing stress fractures during basic training (Beck et al., 1996; Milgrom et al., 1989). Because the size, shape and material properties of adult bones are determined early in life, it will be important to understand the biological processes (or factors) that contribute to variation in these morphometric and material traits in the context of the development of stress fractures. Understanding how the genetic background affects fracture healing will lead to further insights into skeletal tissue response to pharmacological agents that might promote fracture healing and predict if different individuals will heal at differing rates. The hypothesis of these studies is that the genomic processes that lead to the variations in both structural and material properties of bone development will be recapitulated in the developmental mechanism(s) that controls the bone' s structural geometry and material properties during fracture healing. To test this hypothesis, simple transverse fractures were generated in the femora of three strains of mice, A/J, B6, and C3H. These strains of mice were chosen since they have known differences in peak bone mass, which has been related to both structural and material variations intrinsic to these strains. The ultimate goal of this proposal was to identify the genetic components that regulate the variations in development of bone mass and geometry through the comparison of fracture repair processes in the three strains of mice. Two goals were proposed to address the research hypothesis. The objective of goal 1 was to: a) Determine the nature of the quantifiable differences in the biomechanical and microarchitectural properties of the fracture calluses over a 42 day healing period in the three strains of mice. b) Determine how the genetic strain variations in the microarchitectural properties relates to the rates of biomechanical healing as well as the relationship between micro architecture and regain of biomechanical strength. The objective of goal 2 is to: a) Determine the underlying genomic processes that are activated and accompany fracture healing in the three genetic strains of mice and identify strain variation in the patterns of mRNA expression by carrying out both select and full transcriptional profiling of mRNA expression over the same healing period used in aims one b) Identify tissue based differences in the mechanisms and associated genes that are responsible for genetic strain variations in bone development and fracture healing.

BODY

Progress towards completion of Goal 1: Mechanical testing and micro CT has been completed for studies examining all three strains of mice. We revised the end point from 42 days to 35 days, since histological assessments of the 42-day post fracture calluses showed that most of the remodeling in the mouse calluses had been completed and it was decided to initially obtain mechanical and CT properties that would be more reflective of the period of primary bone remodeling and regain in mechanical property versus terminal rates of regain of strength. A series of experiments assessing the biomechanical and structural properties of healing fracture calluses in the three strains of mice described above (A/J, C57/B6, and C3H) were carried out. Two times during fracture healing were initially chosen for examination. Day 21 was chosen since it is one of the earliest times at which mechanical property can be measured and is a key transition point between the endochondral and primary bone formations periods. Day 35 was examined since it is representative of when the bone should have regained its pre fracture strength and is a period of intense secondary formation and remodeling. MicroCT was carried out on between 10-15 calluses per strain per time point and representative microCT images of the three strains at the two time points are presented (Figure 1). MicroCT images show that at 21 days post-fracture, there was significant variation in the size and structure of the calluses among the three inbred mouse strains. The average total area and the polar moment of inertia as quantified from the microCT images of the 21 and 35 days calluses in comparison to the intact bones for A/J, B6, and C3H strains are seen in the lower panels of Fig 6. Significant differences in the size of the calluses were observed among the inbred mouse strains at 21 days. The area and polar moment of inertia of the fracture callus for the A/J mice were 321% and 1022% greater compared to the intact bone. In contrast the area and polar moment of inertia of the B6 mouse fracture calluses were 525% and 2603% greater compared to the intact bone. The area and polar moment of inertia for C3H mice fracture calluses were 484% and 2286% greater compared to the intact bone.

Even more striking however was the variation (all statistically significant) that was seen when these values were compared between mouse strains. The microCT images also showed several striking differences in the quality of the tissue that was formed. The most obvious difference was seen in the lack of bony bridging as exemplified by the area of X-ray translucency in the central region of the C3H calluses at 21 days, which would be indicative of cartilage or fibrous tissue still being present. On the other hand by 35 days all three of the strains of mice showed bony bridging with the C3H mice showing the densest bone. Torsional tests to failure quantitatively validated the visual observations demonstrating that the C3H femurs had a statistically lower mechanical strength and stiffness at 21 days than either the

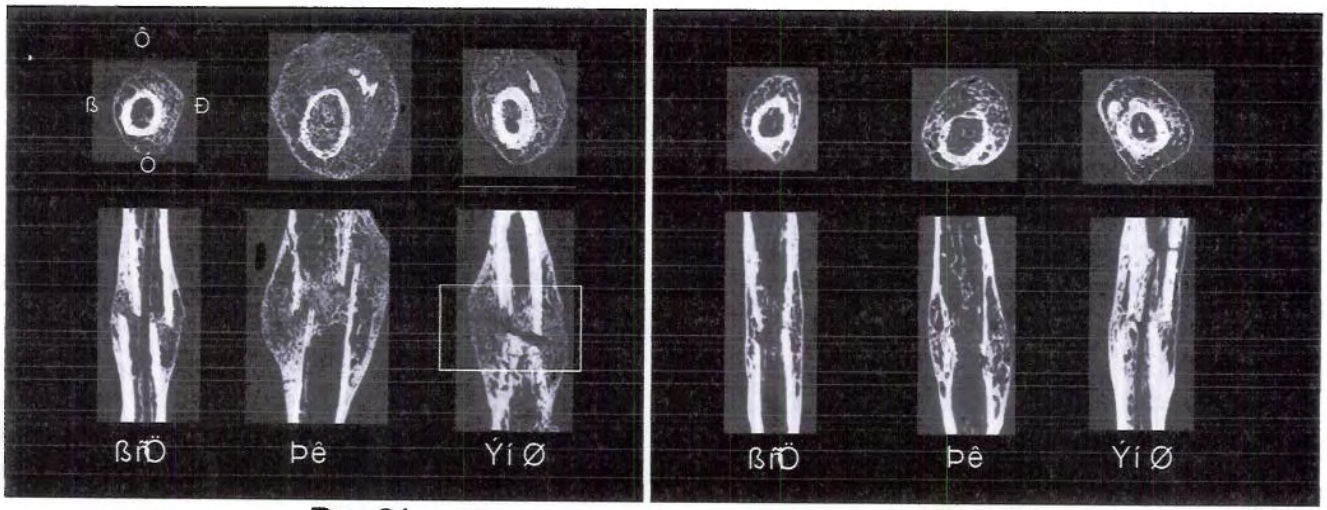

Day 21 Day 35

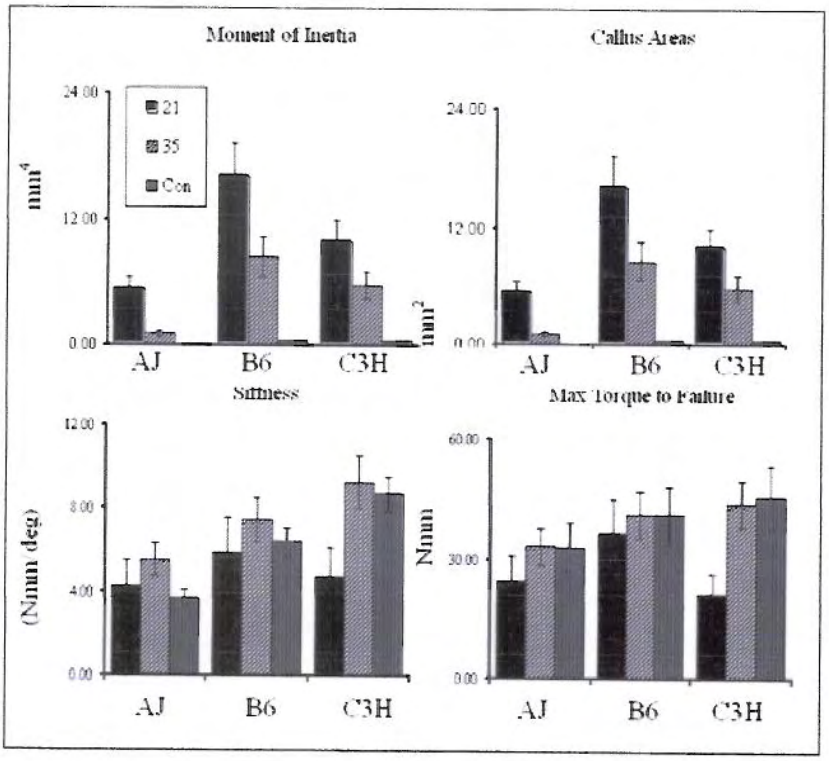

Fig 1. Structural and Biomechanical Comparisons of Fracture Calluses From Three In Bred Strains of Mice.
Upper Panels. Representative microCT images in both transverse and longitudinal orientations taken at 21 and 35 days post fracture. The orientation of the microCT images is denoted for the left most transverse section of the AJ strain. Boxed area of C3H day 21 image shows area that remained unbridged by bone.
Lower Panels. Biomechanical and Structural Data. The data depicted in each of the four panels is denoted.

2 Way Anova For Genotype and Age

Moment of Inertia	p=.0001 p=.0001
Area	p=.0047 p=.0002
Stiffness	p=.0001 p=.0002
Torque to Failure	p=.0194 p=.0002

A/J or B6 mice. Interestingly, the B6 femurs regained their pre-fracture strength by 21 days, which was due to both to the greater cross sectional areas of the callus and the tissue transition to mineralized bone. These data showed then that the mouse with the strongest pre fracture bones (C3H) initially healed the slowest while the B6 mice healed the fastest. *They also clearly show that almost all of the structural features of these three strains of mice are genetically inherited and recapitulated during the processes of fracture healing. More importantly they show that there will be genetic variations in rates of bone healing. This will have eventual clinical importance since as we define these differences in animals this will lead to the development of predictive indices to identify human characteristics that will be diagnostic to variable healing after skeletal trauma.*

Progress towards completion of Goal 2:

The objective of goal 2 were to: a) Determine the underlying genomic processes that are activated and accompany fracture healing in the three genetic strains of mice and identify strain variation in the patterns of mRNA expression by carrying out both select and full transcriptional profiling of mRNA expression over the same healing period used in aims one b) Identify tissue based differences in the mechanisms and associated genes that are responsible for genetic strain variations in bone development and fracture healing. The experiments that are focused on tissue based processes that are related to the genetic variations in bone healing are first discussed.

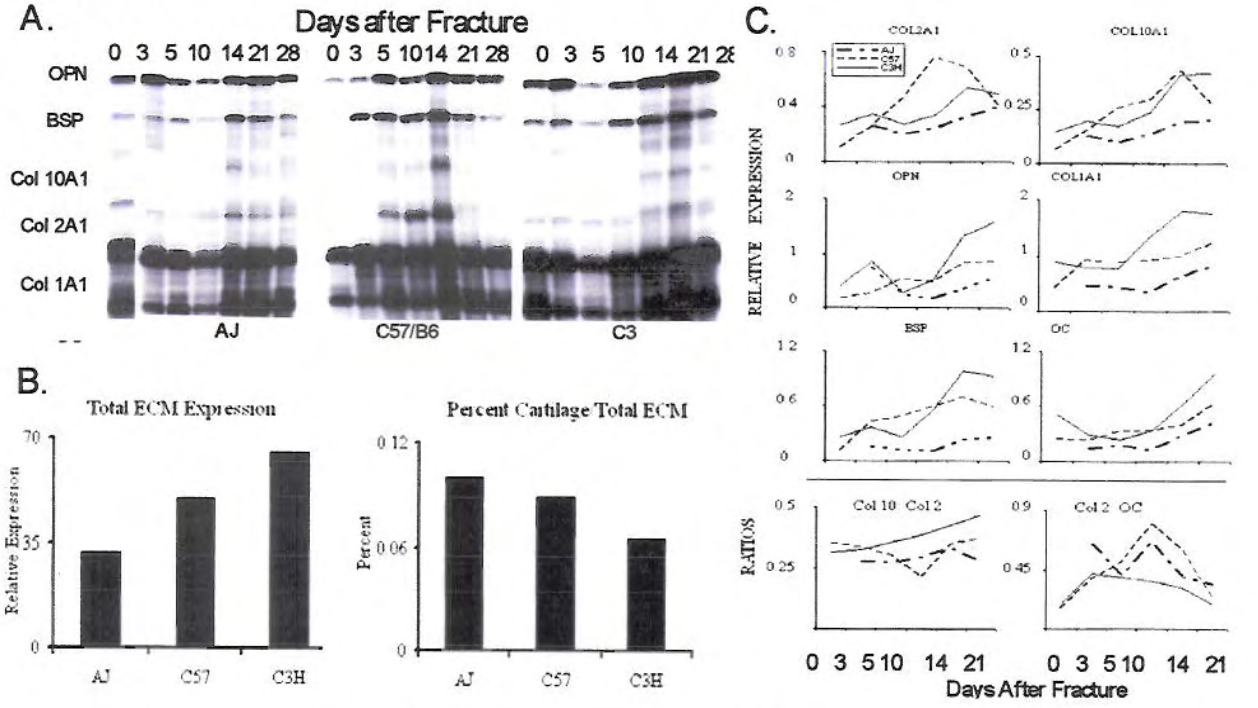

Fig 2. Cartilage and Bone Extracellular Matrix mRNA expression Profiles Across the Time Course of Fracture Healing. **Panel A)** Representative RPA analysis of osteoblast and chondrocyte ECM mRNA expression. The position of the protected bands for each ECM mRNA is denoted in the figure. **Panel B)** Overall anabolic activity was estimated based on direct beta counting of all of the expressed ECM bands normalized to the L32 ribosomal protein housekeeping gene, while the percent cartilage was estmated as the ratio of the total counts of Col10a1 and Col2a1. **Panel C)** Temproal profiles of expression for the expression of individual mRNAs. Each mRNA is denoted in the figure. The Bottom two panels show the ratio of Col10a1:Col2a1 and the Col2a1:Osteocalcin expression.

In order to further define how the underlying genetic difference of the three mouse strains effects the cellular and molecular mechanisms by which fractures heal, we assayed the expression of a group of extracellular matrix mRNAs that would be indicative of either cartilage or bone differentiation and activity. These results are presented in Figure 2. Both a qualitative and quantitative assessment of the mRNA expression data revealed a number of unique features of the extracellular matrix mRNA expression patterns that are informative to the cellular and biological mechanisms that are variable in the three strains of mice. The first and most straight forward observation is the overall differences in anabolic activities between the three strains of mice such that C3H>B6>AJ. As described above, this difference was previously shown in studies of Sheng et al. (2004) in the activity of osteoblasts from mature animals. In the context of the overall types of anabolic activity it is also interesting to note that the percentage of cartilage mRNA expression was highest in the AJ strain and lowest in the C3H strain. This would suggest that in both the AJ and B6 strains that there were greater numbers of mesenchymal stem cells that commit to chondrocytes and progress through an endochondral pathway of bone formation than to an osteoblastic or intramembraneous pathway. This interpretation is also consistent when the ratio of the terminal osteoblast marker osteocalcin was calculated relative to the expression of the cartilage Col2a1 marker (lower right panel). The ratio of Col10a1 to Col2a is also quite informative to the cellular processes that are contributing to fracture healing since it is indicative of the rate of progression of a chondrocyte through endochondral differentiation. In this regard, one of the most interesting aspects of these data was the decreased ratio of Col10a1 to Col2a1 in the B6 calluses preceding a very quick rise at day 14. The A/J calluses also showed a peak in this ratio at day 14, suggesting that the endochondral process is completed soon after day 14. In contrast, the C3H calluses showed a very gradual and continuing increase in the Col10a1 to Col2a1 ratio during the time course that was examined in this study demonstrating that in this strain of mice that the endochondral process takes much longer to complete.

Taking all three sets of data together shows that there is a very large dichotomy of genetic variation in the biological mechanisms by which fracture healing proceeds. In the case of the most rapid rate of healing seen in B6 strain, the process of healing was characterized by a very large expansion of immature chondrocytes as exemplified by the high ratio of cartilage to bone and low ratio Col10a1 to Col2a1, followed by a very rapid rate of hypertrophic differentiation. In contrast in very slowly healing C3H mice the ratio of cartilage to bone was the lowest and rate of hypertrophic maturation was the slowest. In summary then rapid healing was achieved by having a robust endochondral mechanism that was manifested structurally in a large cross sectional callus area and the rapidity of progression through the endochondral phase. In contrast the slowest healing C3H mice had the least endochondral development and only slowly progressed through the endochondral phase, seen grossly in the delay in bony bridging and very low stiffness of the tissue at 21 days. Even though the cross sectional of area of the C3H mice was substantially greater than that of the A/J strain the increased cross sectional area of the callus tissue failed to achieve increased strength and thus healed slower largely because of the poorer material property of the callus due to the persistence of the endochondral cartilage and the more rapid progression of the endochondral process in the A/J and B6 strains. Examination of 14 day post birth growth plates demonstrated similar temporal patterns of endochondral progression with the AJ and B6 mouse strains showing substantially advanced stages of maturation as compared to C3H that lagged behind. These data suggested that the genetic elements, which control the primary structural attributes of bone quality, are recapitulated during fracture healing and can be easily assessed in the temporal window of fracture healing. *These data indicate that the basic temporal and quantitative attributes of endochondral bone formation during fracture healing are genetically regulated.* Finally, we show that the rate of bone healing is not simply related to variability in bone quality but is also controlled by other factors associated with genetic variability intrinsic to endochondral bone formation.

These data drive home the conclusion that the much slower healing of the C3H mice was due to intrinsic genetic variability in biological mechanisms that effected the healing. They also suggest that a number of the underlying mechanisms controlling the genetic variations of bone quality may be observable in the biological processes of fracture healing. These results have been presented in three abstracts included as appended documents 1-3. We have also used funding from this contract to partially support work reported in the Appended manuscript 6. These studies establish the basic methodology to collect histological assessments from fracture calluses as well as demonstrate that callus formation is asymmetrical to the fracture and unique to developmental growth the bone that was fractured. Thus a femur which grows from the distal epiphyisis will have a callus that forms asymmetrically with most of the endochondral bone formation on the distal side. In contrast the tibia that grows from its proximal end has callus that form endochondral bone proximal to the fracture.

A major focus of goal 2 was to carrying out large scale transcriptional profiling comparisons between the three strains. A brief summary of our initial studies establishing transcriptional profiling analysis across fracture healing in the C57/B6 strain are presented in appendix 5. The micro array experiment of the comparison of the three strains has been technically completed, but data analysis is proceeding now and will continue after the contract is finished throughout much of 2006)

Key Research Accomplishments

1) The data validate our hypothesis that the genetic variability that leads to the differences in the quantifiable traits that effect bone quality, also lead to specific quantifiable differences in the mechanisms by which a fractured bone heals.
2) The data identify two genetic extremes of a slow and fast fracture healer, that can be used in our studies.
3) The data demonstrate that assay of complex patterns of mRNA expression has the sensitivity to detect and define variations in biological processes that are genetically inheriable (as an example, variations in patterns of endochondral progression).

Reportable Outcomes

Abstracts

Jepsen KJ, Price C, Nasser P, Alapatt M, Stapleton SN, Silkman L, Kakar S, Einhorn TA, Gerstenfeld LC. Genetic Diversity of Skeletal Ontogeny Is Recapitulated During Fracture Healing. Presented at the 27th Annual Meeting of the American Society for Bone and Mineral Research. Nashville, Tennessee, USA. September 23-27, 2005. **(POSTER) – Appendix 1.**

Stapleton S, Malouf D, Hindson D, Jepsen KJ, Price C, Gerstenfeld LC. Genetic Variability in Osteoclast Activity and 3-Dimensional Spatial Distribution Within 14 Day Post Birth Femurs. Presented at the 27th Annual Meeting of the American Society for Bone and Mineral Research. Nashville, Tennessee, USA. September 23-27, 2005. **(POSTER) – Appendix 2.**

Stapleton S, McLean J, Malouf D, Hindson D, Price C, Jepsen KJ, Gerstenfeld LC. Genetic Variation in the Osteoclast Activity and Spatial Distribution During Growth and Modeling of Long Bones as Assessed by 3-Dimensional Reconstruction. Presented at the 52nd Annual Meeting of the Orthopaedic Research Society. Chicago, Illinois, USA. March 19-22, 2006. **(POSTER) – Appendix 3.**

Jepsen KJ, Price C, Nasser P, Hu B, Alapatt M, Silkman L, Stapleton S, Kakar S, Einhorn TA, Gerstenfeld LC. Genetic Variability in the Rate of Fracture Healing Within Inbred Strains of Mice Reveals Basic Genetic Differences in the Rates of Epiphyseal Growth. Presented at the 52nd Annual

Meeting of the Orthopaedic Research Society. Chicago, Illinois, USA. March 19-22, 2006. **(POSTER) – Appendix 4.**

Papers

Wang K, Vishwanath P, Eichler G, Edgar C, Einhorn TA, Smith T, Gerstenfeld LC. Analysis of Fracture Healing by Large Scale Transcriptional Profile Identified Temporal Relationships Between Metalloproteinase and ADAMTS mRNA Expression. Matrix Biology, submitted. – **Appendix 5.**

Gerstenfeld LC, Alkhiary YM, Krall EA, Nicholls FH, Stapleton SN, Fitch JL, Tsay AW, Graves DT, Jepsen KJ, Einhorn TA. Three Dimensional Reconstruction of Fracture Callus Morphogenesis Demonstrate Asymmetry in Callus Development. Journal of Bone and Mineral Research, submitted. – **Appendix 6.**

There is a minimum of four full length articles that will be written in 2006 that are derivative from this work. I will be happy on request to submit these completed manuscripts and final citations of this work as it is published.

Conclusions

1. Genetic variability in bone quality is recapitulated during bone healing.

2. Genetic variability in bone quality is relatable to variations in rates of bone healing.

3. Genetic variability in rates of bone healing appears to be due to genetic differences in endochodrnal developmental growth.

4. The identification of specific types of structural and biomechanical traits that are both relatable to rates of fracture healing and specific biological processes that occur during fracture healing have the potential in an intermediate period of time (2-five years) to be developed into clinically usable assays that are prognostic of slow or fast fracture healing and of at risk to fracture bone quality to stress fractures.

References

Beck TJ, Ruff CB, Mourtada FA, Shaffer RA, Maxwell-Williams K, Kao GL, Sartoris DJ, Brodine S. 1996. Dual-energy x-ray absorptiometry derived structural geometry for stress fracture prediction in male U.S. Marine Corp recruits. J Bone Miner Res, 11:645-653.

Milgrom C, Giladi M, Simkin A, Rand N, Kedem R, Kashtan H, Stein M, Gomori M. 1989. The area moment of inertia of the tibia: A risk factor for stress fractures. J Biomech, 22:1243-1248.

Jepsen KJ, Pennington DE, Lee Y-L, Warman M, Nadeau J. Bone brittleness varies with genetic background in A/J and C57BL/6J inbred mice. J Bone Miner Res. 2001; 16(10):1854-1862.

Sheng MH, Lau KH, Beamer WG, Baylink DJ, Wergedal JE. In vivo and in vitro evidence that the high osteoblastic activity in C3H/HeJ mice compared to C57BL/6J mice is intrinsic to bone cells. Bone. 2004; 35(3):711-719.

Appendices

Appendix 1. Jepsen KJ, Price C, Nasser P, Alapatt M, Stapleton SN, Silkman L, Kakar S, Einhorn TA, Gerstenfeld LC. Genetic Diversity of Skeletal Ontogeny Is Recapitulated During Fracture Healing. Presented at the 27th Annual Meeting of the American Society for Bone and Mineral Research. Nashville, Tennessee, USA. September 23-27, 2005.

Appendix 2. Stapleton S, Malouf D, Hindson D, Jepsen KJ, Price C, Gerstenfeld LC. Genetic Variability in Osteoclast Activity and 3-Dimensional Spatial Distribution Within 14 Day Post Birth Femurs. Presented at the 27th Annual Meeting of the American Society for Bone and Mineral Research. Nashville, Tennessee, USA. September 23-27, 2005.

Appendix 3. Stapleton S, McLean J, Malouf D, Hindson D, Price C, Jepsen KJ, Gerstenfeld LC. Genetic Variation in the Osteoclast Activity and Spatial Distribution During Growth and Modeling of Long Bones as Assessed by 3-Dimensional Reconstruction. Presented at the 52nd Annual Meeting of the Orthopaedic Research Society. Chicago, Illinois, USA. March 19-22, 2006.

Appendix 4. Jepsen KJ, Price C, Nasser P, Hu B, Alapatt M, Silkman L, Stapleton S, Kakar S, Einhorn TA, Gerstenfeld LC. Genetic Variability in the Rate of Fracture Healing Within Inbred Strains of Mice Reveals Basic Genetic Differences in the Rates of Epiphyseal Growth. Presented at the 52nd Annual Meeting of the Orthopaedic Research Society. Chicago, Illinois, USA. March 19-22, 2006.

Appendix 5. Wang K, Vishwanath P, Eichler G, Edgar C, Einhorn TA, Smith T, Gerstenfeld LC. Analysis of Fracture Healing by Large Scale Transcriptional Profile Identified Temporal Relationships Between Metalloproteinase and ADAMTS mRNA Expression. Matrix Biology, submitted.

Appendix 6. Gerstenfeld LC, Alkhiary YM, Krall EA, Nicholls FH, Stapleton SN, Fitch JL, Tsay AW, Graves DT, Jepsen KJ, Einhorn TA. Three Dimensional Reconstruction of Fracture Callus Morphogenesis Demonstrate Asymmetry in Callus Development. Journal of Bone and Mineral Research, submitted.

Appendix 1

Genetic Diversity of Skeletal Ontogeny Is Recapitulated During Fracture Healing

K. J. Jepsen[1], C. Price[1], P. Nasser*[1], M. Alapatt*[2], S. N. Stapleton[2], L. Silkman*[2], S. Kakar[2], T. A. Einhorn[2], L. C. Gerstenfeld[2]

[1]Department of Orthopaedics, Mount Sinai School of Medicine, New York, NY, USA, [2]Orthopaedic Surgery, Boston University Medical Center, Boston, MA, USA.

Microarchitecture (microCT) and mechanical properties (torque to failure) were examined over 35 days of fracture healing in A/J, C57BL/6J (B6), and C3H/HeJ (C3H) inbred strains of mice. These studies demonstrated that the major architectural characteristics of bone quality (moment of inertia, cortical area, trabecular volume), which varied significantly among the strains, were recapitulated during fracture healing. The strain having the highest pre-fracture strength (C3H) however regained this property the slowest. Both micro-CT analysis and the temporal expression patterns of cartilage versus bone mRNAs demonstrated very slow (> 2 wk delay) cartilage resorption for C3H compared to B6. This was due to the slower transit of C3H bones through the endochondral phase. Furthermore, this slower transit time could be related to genetic variability in the rate of endochondral maturation based on the 5-7 day difference in times of peak chondrocyte hypertrophy based on Col10A1 expression. Quantitative analysis of the expression of both cartilage and bone extracellular matrix mRNAs showed a direct correlation between the total anabolic activity of a given strain of mouse and the overall volume of bone tissue formed such that (C3H>B6>AJ). Examination of 14 day post birth growth plates demonstrated similar temporal patterns of endochondral progression with the AJ and B6 mouse strains showing substantially advanced stages of maturation as compared to C3H that lagged behind. These data suggested that the genetic elements, which control the primary structural attributes of bone quality, are recapitulated during fracture healing and can be easily assessed in the temporal window of fracture healing. These data indicate that the basic temporal and quantitative attributes of endochondral bone formation during fracture healing are genetically regulated. Finally, we show that the rate of bone healing is not simply related to variability in bone quality but is also controlled by other factors associated with genetic variability intrinsic to endochondral bone formation.

Appendix 2

Genetic Variability in Osteoclast Activity and 3-Dimensional Spatial Distribution Within 14 Day Post Birth Femurs

S. Stapleton*, D. Malouf, D. Hindson, K. J. Jepsen,+ C. Price,+ LC Gerstenfeld*
*Orthopaedic Research Laboratory, Boston University Medical Center, Boston, MA 02118-2526, USA, Department of Orthopaedics, Mount Sinai School of Medicine, New York, New York 10029-6574, USA.

Numerous studies have shown that variation in bone morphology in different inbred strains of mice is genetically determined. The genetic variation is reflected in different rates of formation and resorption on endosteal vs. periosteal surfaces; the relative amount and location of cellular activities thus determining the relationship between bone size and the mechanical demands imposed by weight bearing during growth. A quantitative measure of osteoclast numbers and their 3-dimensional spatial distribution were assessed in A/J, C57BL/6J (B6), and C3H/HeJ (C3H) strains of mice. Transverse serial sections were taken at 100 micron increments along the length of femurs from 14 day mice and stained for osteoclast activity. Serial sections were arranged in stacks and the 3-D spatial distribution of osteoclasts within the femurs was reconstructed (AJ and C3H are presented). Renderings of the bone in differing longitudinal planes, or for TRAP activity alone, were examined. Moving distally along the femur revealed an approximate 50/50 distribution of TRAP staining on both endosteal and periosteal surfaces within AJ and B6 femurs, but no discernable pattern for C3H. The AJ strain, which has the smallest bone mass, had the highest level of TRAP activity with the majority of the enzyme activity seen either on the periosteal or opposing endosteal surfaces (compare the distribution of the pattern of dark grey coloring that denotes areas of TRAP activity). For the B6 strain, which had the next highest level, most of the activity was either intracortical or on trabecular bone in the medullary space; much less staining visualized on the bone surfaces. Interestingly, this strain has the thinnest cortices and largest medullary space. TRAP staining in the C3H animals was almost unobservable when viewed in the reconstructions and this strain has both the thickest cortices and highest bone mass. These data demonstrate profound differences, in both the quantity and spatial characteristics of osteoclastic activities, in different strains of inbred mice. This suggested that both these features of cellular activity are relatable to spatial geometry and overall mass of a bone and are genetically regulated.

Appendix 3

GENETIC VARIATION IN THE OSTEOCLAST ACTIVITY AND SPATIAL DISTRIBUTION DURING GROWTH AND MODELING OF LONG BONES AS ASSESSED BY 3-DIMENSIONAL RECONSTRUCTION

+*Stapleton, S; *McLean, J; *Malouf, D; *Hindson, D; **Price, C; **Jepsen, KJ; *Gerstenfeld, LC
*Orthopaedic Research Laboratory, Boston University Medical Center, Boston, MA 02118-2526, USA
**Department of Orthopaedics, Mount Sinai School of Medicine, New York, New York 10029-6574, USA.
snstaple@bu.edu

INTRODUCTION

Bone quality has been shown to be controlled by multiple genes that regulate skeletal tissue structure. One set of genes effects geometrical features such as cortical and trabecular thickness, cross sectional areas and trabecular numbers while a second, not necessarily independent, set of genes affects tissue material properties inclusive of mineral content and organic matrix composition (1). At the cellular level these genetic variations are reflected in different rates of formation and resorption on endosteal and periosteal surfaces versus amount of remodeling in cortical and trabecular bone. Thus, the relative amount and location of cellular activities is a large determinant of many of the geometric features of skeletal tissues and is responsive to the mechanical demands imposed by weight bearing during growth. In this study a quantitative measure of the spatial distribution of osteoclast activity was assessed in three strains of inbred male mice (A/J, C57BL/6J [B6], and C3H/HeJ [C3H]),which have varying bone qualities. The distribution of osteoclast activity was compared relative to the overall endochondral and osseous growth of these tissues as determined by three dimensional histological reconstruction of the femurs of these mice.

MATERIALS AND METHODS

Five micron transverse sections were generated from intact fourteen day decalcified and paraffin embedded mouse femurs. Sections were taken at 100 micron increments across the entire length of the femur and safranin-O fast green staining was used to distinguish mature cartilage from bone and other connective tissues. Osteoclast activity was detected by the use of TRAP staining. Sections were then photographed at 40X and loaded into Adobe Photoshop for editing. Images were aligned with each other and pertinent tissues identified. Bone and cartilage were distinguished by hand tracing, and TRAP stained cells were located by pixel value. All sections were false colored according to type of tissue that was being assessed and then converted into grey scale. Amira 3.0 software system (Visual Concepts GmbH, Company, Konrad-Zuse-Zentrum (ZIB), Research Institute Berlin, Germany) was used for 3D visualization and data analysis. All image modifications were performed in Adobe Photoshop Software, (Adobe Systems, Incorporated; San Jose, CA USA). Areas of TRAP activity were calculated by use of the surface area function in Amira 3.1 within each of the reconstructed models. Areas and spatial distribution of TRAP activity was further analyzed by selective cell counts of individual osteoclasts on specific anatomical surfaces.

RESULTS

Analysis of the three strains of femurs showed that there was an approximate 50/50 distribution of TRAP staining on both endosteal and periosteal surfaces within AJ and B6 femurs within the center diaphyseal regions of the bone, but that no discernable pattern was seen for C3H (Figure 1). The AJ strain, which has the smallest bone mass, had the highest level of TRAP activity with the majority of the enzyme activity seen either on the periosteal or opposing endosteal surfaces (compare the distribution of the pattern of dark grey coloring that denotes areas of TRAP activity). For the B6 strain, which had the next highest level, a pattern similar to AJ resulted, but with less staining visualized on the bone surfaces. Interestingly, this strain has the thinnest cortices and largest medullary space with the greatest number of cells seen in the intramedullary space. TRAP staining in the C3H animals was almost unobservable when viewed in the reconstructions and this strain has both the thickest cortices and highest bone mass. An analysis of the actual TRAP stained area (Figure 2) and cells also showed varying quantitative results between the three strains of mice

An examination of the progression of endochondral tissue maturation in the three strains demonstrated that the AJ stains had the most progressed endochondral maturation, B6 strain was intermediate and the C3 had the least. In situ hybridization with Type II collagen validated strain specific variation in chondrocyte metabolic activity, and an assessment of cellular numbers within growth plate columns showed that the AJ strain had the greatest cell number per column and largest column heights while the C3 mice had the smallest number of cells and shortest columns.

DISCUSSION

These data demonstrate profound differences, in both the quantity and spatial characteristics of osteoclastic activities, in different strains of inbred mice. These data suggest that both these features of osteoclast activity are relatable to spatial geometry and overall mass of a bone and are genetically regulated. Data examining the epiphyseal growth plates suggested that there is also genetic variation in the rate of linear growth that is associated with the rate of endochondral chondrocyte maturation such that the AJ showed the fastest rate of growth and cartilage maturation while the C3H had the slowest rate and cartilage maturation. These data pose specific questions as to whether there is an association between the smaller transverse bone areas and the rate of liner bone growth, and what are the molecular mechanisms of linkage between transverse and linear growth.

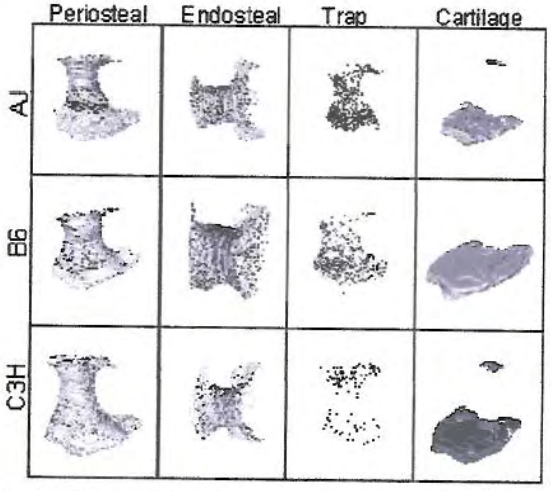

Fig 1. Spatial Orientation of modeling and endochondral cartilage development in inbred strains of mice. Three views (left to right) of the reconstructed spatial distribution of TRAP (osteoclast) activity in the bone in the 3 strains of mice. The bone is modeled in light gray and the TRAP activity is modeled in black. The left view depicts the periosteal surface. The middle view is a cut away looking onto the endosteal

surface. The right view depicts the entire volume that was sampled for TRAP staining without the superposition of the reconstruction of the bone surfaces. The far right panel models the mature cartilage (light grey) and immature cartilage (black) within the growth plates

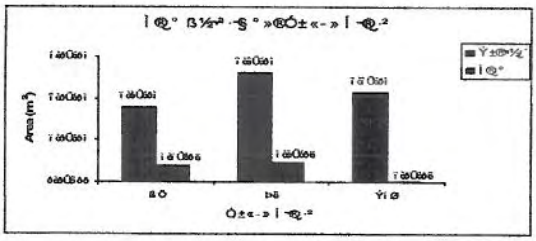

Fig 2. Catabolic activity per bone area in AJ, B6 and C3H mice Area calculations based on TRAP staining in three strains of mice.

1. Jepsen et al .J Bone Miner Res. 2001; 16(10):1854-1862

Appendix 4

GENETIC VARIABILITY IN THE RATE OF FRACTURE HEALING WITHIN INBRED STRAINS OF MICE REVEALS BASIC GENETIC DIFFERENCES IN THE RATES OF EPIPHYSEAL GROWTH

**K. J. Jepsen; **C. Price; **P. Nasser; **B. Hu; *M. Alapatt; *L. Silkman; *S. Stapleton; *S. Kakar; *T. A. Einhorn; +*L. C. Gerstenfeld
*Orthopaedic Research Laboratory, Boston University Medical Center, Boston, MA 02118-2526, USA
**Department of Orthopaedics, Mount Sinai School of Medicine, New York, New York 10029-6574, USA.
lgersten@bu.edu

INTRODUCTION

Fracture healing is a specialized post-natal repair process that recapitulates many aspects of embryological skeletal development. Recent studies using inbred strains of mice have shown that bone quality is controlled by multiple genes that regulate skeletal tissue structure. Because many of the molecular mechanisms that control cellular differentiation and growth during embryogenesis are recapitulated during fracture repair, we tested the hypothesis that the rate of fracture healing will vary with genetic background. We further tested whether genetic variability in fracture repair may have its origins in variable endochondral bone formation processes by comparing the cellular behavior during fracture repair with the cellular behavior of the growth plate. In this study three strains of inbred mice with varying bone qualities (A/J, C57BL/6J [B6], and C3H/HeJ [C3H]) were fractured and the rate of regain of mechanical properties was assessed. Basic histological and molecular features across fracture healing were used to measure rates of chondrogenic and osteogenic differentiation. These studies revealed that the overall anabolic activity of skeletal tissues is genetically controlled and that rates of chondrocyte maturation during endochondral bone formation also show genetic variation that affect rates of healing. These observations led to comparisons of the rates of chondrogenic differentiation during post-natal epiphyseal bone growth that validated basic genetic differences in skeletal tissue development.

MATERIALS AND METHODS

Simple transverse mid-diaphyseal femur fractures were generated in 8 to 10 week old male A/J, C57BL/6J [B6], and C3H/HeJ [C3H] mice as previously described (1). Fracture calluses were harvested at 21 and 35 days for torsion mechanical testing and microCT analysis. Callus tissues were harvested at multiple post-fracture time points over a 28 day period for mRNA and histological measurements. The respective distal and proximal epiphyseal growth plates of tibia and femurs from 14 day old (post birth) mice were histologically examined. Type II and X collagen mRNA expression analysis was assessed by in situ hybridization and mRNA expression within the whole tissue was assessed by ribonuclease protection analysis.

RESULTS

Microarchitecture (microCT) and mechanical properties (torque to failure) were examined at 21 and 35 days of fracture healing in A/J, C57BL/6J (B6), and C3H/HeJ (C3H). These studies demonstrated that the major architectural characteristics of bone quality (moment of inertia, cortical area, trabecular volume), which varied significantly among the strains, were recapitulated during fracture healing (Figure 1). The strain having the highest pre-fracture strength (C3H) however regained its strength the slowest as based on torque to failure measurements. Both micro-CT analysis (seen as x-ray lucency) and the temporal expression patterns of cartilage versus bone mRNAs demonstrated very slow (≥ 2 wk delay) cartilage resorption for C3H compared to either B6 or AJ. This was due to the slower transit of C3H bones through the endochondral phase based on the ratios of Col2a1 to Col10a1 expression that were used as a measure of the progresion of hypertrophic chondrocyte differentiation (Figure 2). Furthermore, this slower transit time could be related to genetic variablity in the rate of endochondral maturation based on the 5-7 day difference in times of peak chondrocyte hypertophy based on Col10A1 expression. Quantitative analysis of the expression of both cartilage and bone extracellular matrix mRNAs further showed a direct correlation between the total anabolic activity of a given strain of mouse and the overall volume of bone tissue formed such that (C3H>B6>AJ).

Examination of 14 day post birth growth plates demonstrated similar temporal patterns of endochondral progression with the AJ and B6 mouse strains showing substantially advanced stages of maturation as compared to C3H which lagged behind. This is seen in Figure 3 of the in situ hybridization of the femoral growth plates that showed the associated genetic variablity in overall Col2a1 expression intrinsic to the differring strains of mice. The progression of endochondral tissue was markedly different in that AJ stains had the most progressed endochondral maturation with B6 strain being intermediate and the C3 had the least. Cellular numbers within growth plate columns also showed that the AJ strain had the greatest cell number per column and largest column heights while the C3 mice had the smallest number of cells and shortest columns.

DISCUSSION

These data suggested that the genetic elements which control the primary structural attributes of bone quality are recapitulated during fracture healing and can be easily assessed in the temporal window of fracture healing. These data indicate that the basic temporal and quantitative attributes of endochondral bone formation during fracture healing are genetically regulated. Finally, we show that the rate of bone healing is not simply related to variability in bone quality but is also controlled by other factors

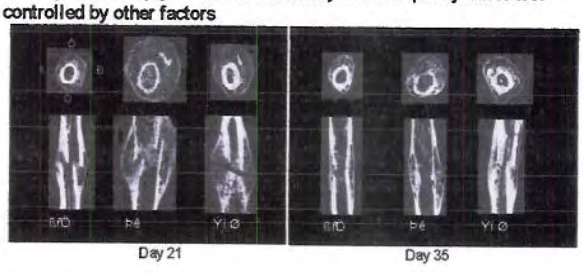

Fig 1. Structural and Biomechanical Comparisons of Fracture Calluses From Three Inbred Strains of Mice. Representative microCT images in both transverse and longitudinal orientations taken at 21 and 35 days post fracture. The orientation of the microCT images is denoted for the left most transverse section of the AJ strain. Boxed area of C3H day 21 image shows area that remained unbridged by bone.

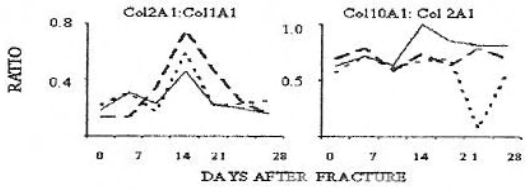

Fig 2 Ratios of Bone to Cartilage and Hypertrophic Cartilage Maturation Over Time Course of Fracture Callus Healing.
The measured ratios of individual collagen mRNA expression are denoted in the figure. Solid line =C3H, Dotted line AJ, Dashed line B6.

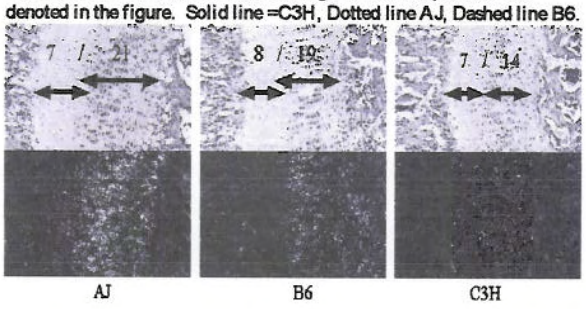

Fig 3 Comparison of Distal Femur Growth Plates at 14 Days Post Birth. Upper panel are light level images of representative areas from the growth plates of the three strains of mice. Lower panels showed dark field images from the in situ hybridizations with Col2A1 probes. Staggered arrows show the variation in column sizes of the hypertrophic and growth zones of the three strains. Numbers are simple counts of cells seen in the two zones.

1. Kon et al . J Bone Miner Res. 2001; 16:1004-1014.

Appendix 5

Analysis of Fracture Healing by Large Scale Transcriptional Profile Identified Temporal Relationships Between Metalloproteinase and ADAMTS mRNA Expression

Kevin Wang[1], Prashanth Vishwanath[2], Gabriel S. Eichler[2], Maisa O. Al-Sebaei[1,3] Cory M. Edgar[1], Thomas A. Einhorn[1], Temple F. Smith[2], and Louis C. Gerstenfeld[1*]

[1]Department of Orthopaedic Surgery, Orthopaedic Research Laboratory, Boston University Medical Center, Boston, MA

[2]Department of Biomedical Engineering, Boston University School of Engineering, Boston MA

[3]Department of Oral & Maxillofacial Surgery, Boston University School of Dental Medicine, Boston, MA

*Corresponding author:
Louis C. Gerstenfeld, Ph.D.
Boston University Medical Center
Department of Orthopaedic Surgery
Orthopaedic Research Laboratory
715 Albany Street, R-205, Boston, MA 02118
E-mail: lgersten@bu.edu
Phone: 617-414-1660
Fax: 617-414-1661

Abstract

The aim of this study was to validate the use of transcriptional profiling as a means of characterizing the complex interactions of the thousands of genes that are expressed during fracture healing. Standard mid-diaphyseal tibia fractures were generated in C57/B6 murine tibiae and the transcriptional expression of ~13,000 genes was assessed. Three time points after fracture were assessed: day three, representative of the inflammatory phase; day 10, representative of the peak of cartilage formation; and day 21, representative of the period of primary bone formation and coupled remodeling. A self-organizing mapping approach of the data revealed the temporal relationships between the expression of mRNAs for extracellular matrix proteins and the proteases that degrade the proteoglycan and collagenous matrices. A broad group of extracellular matrix protein mRNAs representative of basement membranes, blood vessels and cartilage all showed elevated expression over the first 21 days of fracture healing. The sorting of the data identified an orderly temporal expression of the metalloproteinases and ADAMTS during the progression of fracture healing with (MMP2/MMP14/TIMP2) and ADAMTS 4 and 15 preceding the expression of (MMP9/MMP13). Based on their patterns of expression, relative to the known activities of the encoded proteolytic enzymes, our results suggest that the dissolution of cartilage protoeglycans proceeds before the underlying collagenous components of the matrix are removed. The exclusion of several mRNAs that are normally expressed by osteoclasts in the profiles of mRNAs from days 3 and 10 suggests that osteoclastic activity was largely absent during the early periods of cartilage tissue formation and that proteoglycan and specific collagenase activities, precedes or is prerequisite to later osteoclast infiltration into the remodeling tissues.

Keywords: MMP, ADAMTS, Fracture Healing, Transcriptional Profiling

1. Introduction

Osseous skeletal tissues are one of the few tissues in adult vertebrate animals that regenerate in response to injury. Fracture healing encompasses the complex interaction of multiple cell types and many different biological processes (Ferguson et al., 1999; Gerstenfeld et al., 2003b; Vortkamp et al., 1998). Thus fracture healing is a unique model to identify the relationships between the mechanisms that regulate specific responses to a traumatic injury and the genetic components that control the development of bone. The identification and understanding of interactions of the various genomic components that both respond to injury, affect bone development and regulate repair are therefore of considerable clinical importance. Identifying these molecular mechanisms may help us develop predictive indices for the rates of fracture healing that are based on specific biological processes. These data will also be informative to potential therapeutic interventions that may promote bone healing.

Many previous studies of fracture healing have focused on the activities of individual genes that are of functional importance during the differentiation of skeletal cell types. The biological complexity of fracture healing, however suggests that it is regulated by hundreds, if not thousands, of transcriptionally regulated genes. These genes are expressed by both skeletal and non skeletal cell types and they are involved in multiple biological processes that facilitate bone healing. In order to understand how the activities of such a large number of genes are coordinated, and how their activities are associated with a given cellular or biological process, recent innovations in the ability to analyze genome wide transcriptional activities can be used (Hadjiargyrou et al., 2002; Desai et al., 2003). Such approaches enable the transcriptional activities of large numbers of genes to be assessed and the complex interactions of genes to be organized and visualized in an understandable and interpretable manner.

The aim of this study was to validate the use of transcriptional profiling as a means of characterizing the complex interactions of approximately 13,000 genes that are expressed during fracture healing. A simplified study design using a limited set of time points that would delineate the inflammatory, endochondral (cartilage), and primary bone formation phases of fracture healing was carried out. This study selectively focused on the complement of extracellular matrix proteins and the two primary proteolytic enzyme families (metalloproteinases and ADAMTs) that are responsible for remodeling extracellular matrices. This analysis identified several

hundred expressed genes that showed significant differential expression compared to unfractured bones. Clustering analysis identified specific groups of metalloproteinases and ADAMTS mRNAs and placed their expression in context to the expression of specific mRNAs associated with cartilage, bone and osteoclast cell functions.

2. Results

The expression of a group of extracellular matrix protein mRNAs that is representative of cartilage and bone formation was first assessed in each set of RNAs that was used for transcriptional profiling. Ribonuclease protection analysis was carried out in order to ensure that each RNA sample was representative of the inflammatory, cartilage and bone formation phases of fracture healing (Figure 1). The inflammatory phase of fracture healing (day 3), was characterized by an initial decrease in the expression of the major mRNA markers of differentiated osteogenic cells (osteocalcin type I collagen and bone sialoprotein). As previously shown, this is due to the large influx of non osteogenic cells within the hematoma that forms in response to the fracture (Kon et al., 2001). At this time large numbers of skeletogenic precursors that contribute to the initial repair tissue are recruited but do not yet express a skeletal tissue phenotype. Consistent with this interpretation was the increased expression of osteopontin that is expressed by macrophages and other inflammatory cells (Kon et al., 2001), as well as early skeletalgenic precursors (Barnes et al., 1999; Bolander, 1992). Day 10 calluses tissue represents the peak of cartilage formation that takes place during endochondral bone formation (Gerstenfeld et al., 2003a). The restricted nature of the chondrocyte mRNA expression at this time point is exemplified by the high levels of both collagen types II and X mRNA expression. Day 21 is representative both of primary bone formation and coupled remodeling. At this time point, the profile of expressed mRNAs has almost returned to that seen in unfractured bone however the levels of osteocalcin remain considerably elevated above the baseline of normal bone.

While the RPA analysis is an important assessment of RNA integrity and provides a means of confirming the temporal progression of the repair process, microarray experiments necessitate a much higher purity of RNA that may only be empirically determined by carrying out an actual microarray experiment. The raw data from the spot intensities for the expression of osteocalcin was chosen to validate the integrity of the profiling experiments. The expression of this mRNA is known to be one of the most highly restricted to bone, and its expression has

been shown to progressively increase over the time course of fracture healing. The spot intensities for both fluorescent channels from the reciprocal labeling and hybridization of one set of experimental and reference samples are presented. These data show an excellent quantitative correspondence of the increasing intensity of fluorescent readout over the time course of fracture healing, in comparison to the RPA assay.

Using unfractured bone mRNA as the reference to which experimental samples were compared, we used a conservative selection process in which only those mRNAs showing a >log2 difference in expression compared to the levels of expression in unfractured bone would be considered for further analysis. The global representation of these data is summarized as a ratio intensity plot that is depicted in Figure 3. This figure illustrates the total number of observed mRNAs at each time point having a >log2 fold variation from the observed levels in unfractured bone. The conformance of the majority of the spots within 1 SD of their log ratios also provides an excellent index of the overall integrity of the numeric data that was developed from each array (Tamayo et al., 1999; Kohonen and Somervuo, 2002). A comparison of the three graphs shows that the greatest number of genes having >log2 variation lesser or greater expression from unfractured bone were seen at days 3 and 10 days post fracture. Far fewer genes showed such large quantitative differences in their expression relative to unfractured bone by 21 days post fracture. It is interesting to note that as the fracture healed, the complement of genes that were differentially expressed greatly diminished as the bone returns to its pre fracture makeup (Figure 3). Thus the complexity of the number of biological processes that are concurrently operative during the early phases of fracture healing is much greater than that which occurred during the later periods of primary bone formation

The first level of analysis was to identify those expressed mRNAs that are quantitatively different from unfractured bone. A small subset of all of the mRNAs showing differential levels of expression, are presented in Table 2. The primary focus of this table is to highlight expressed mRNAs that are selectively expressed during the three phases of fracture healing, and that are known to be associated with either cartilage formation or osteoclast activity. A number of other mRNAs that encode specific morphogenetic regulators and transcriptional factors are also highlighted in the table. These were included since they have not been previously well characterized during fracture healing but showed strong differences in their expression relative to unfractured bone and may be of general interest.

At day 10 post fracture, very large changes in the expression of perlecan, cartilage oligomeric matrix protein (COMP) and matrix gla protein (MGP) mRNAS were observed. All three of these mRNAs or their proteins are known to be highly expressed in developing cartilage but not in normal bone. Their identification at this time point is consistent with the RPA data for collagen Types II and X and further validates the restricted expression of cartilage associated mRNAs at this time point. On the other hand, a number of enzymes such as carbonic anhydrase 2 and tartrate resistant acid phosphatase that are all known to be expressed at high levels by osteoclasts (Rousselle and Heymann, 2002), were significantly diminished from their reference values in native bone at days 3 and 10 post fracture. The diminished expression of marker mRNAs for osteoclasts was also accompanied by the elevation of two separate antagonist to RANK-L (major regulator of osteoclast differentiation), osteoprotegerin, and TNF super family member 22. A number other mRNAs of interest that were induced early and persisted through out the time course of fracture healing include osteoblast specific factor 2 (fasciclin I-like) OSF-2 and osteoglycin. In references to the expression of OSF-2 and osteoglycin both these genes have all been identified in two separate large scale in vitro transcriptional profiling studies that were focused on identifying genes within mesenchymal stem cells that are regulated by BMPs (Balint et al., 2003; Stock et al., 2004).

The first stage of the analysis only identified candidate genes of interest based on changes in their quantitative levels of expression. In the second stage of this analysis bioinformatics approaches were applied to identify functional groupings of genes. A self-organizing mapping (SOMs) approach was used to identify the temporal patterns of expression for two groups of proteolytic enzymes (MMPS, ADAMTS) and the extracellular matrix protein mRNAs. Table 3 presents the two groupings of extracellular matrix protein mRNAs that showed slightly different temporal patterns of expression but which were grouped closely together in the two dimensional graphical analysis of the SOMs (data not shown). Both groups of these mRNAs show increased levels of expression over unfractured bone at all of the time points. The Group 1 mRNAs showed an increasing level of expression between 3 and 14 days after which their levels began to fall. This group of mRNAs included those encoding proteins found mainly in basement membranes and vascular elements, a second set of mRNAs primarily encoding proteins found in cartilage, and a third group of mRNAs for proteins found in many different connective tissues. Group II mRNAs had a pattern of expression that showed a continuous increasing level of expression

across the entire time course and included mRNAs encoding both α1 and α2 polypeptides of type I collagen. Interestingly, the mRNAs encoding several different metalloproteinase were one of a several functional groups of expressed mRNAs that were identified without prior selection and based solely on their strong quantitative differences in expression. The identification of multiple MMPs that are involved in both vascularization and collagenous tissue proteolysis was of considerable interest, since the resorption of cartilage tissue and tissue vascularization represents two of the major transitional processes of endochondral bone formation (Vu et al., 1998; Zho et al., 2000; Street et al., 2002; Ortega et al., 2003). These observations led us to subsequently use SOMs to further examine the temporal relationships between the metalloproteinases and the ADAMTS proteases that are known to degrade proteoglycans. A graphical presentation for MMPs and TIMPs are presented in Figure 4. Individual groups of MMP mRNAs showed varying temporal patterns of expression, with the expression of MMPs 14 and 2 preceding that of MMP 9 and MMP 13. In contrast, the expression of MMPs 8 and 19 showed a strong inhibition in their expression over the 21 days of bone healing. The metalloproteinase inhibitors (TIMPs 2 and 3) had an almost identical pattern of expression as MMPs 2 and 14 while TIMP1 was induced early after fracture and remained highly expressed thereafter.

Specific members of the ADAMTS proteases gene family also showed unique temporal patterns of expression across the time course of fracture (Figure 5). ADAMTS 4 and 15, which both have aggrecanases activity (Apte, 2004), paralleled the expression of MMPs 2 and 14. On the other hand, ADAMTS 1 which also has potential aggrencanase activity followed the pattern of expression of MMPs 9 and 13. The final ADAMTS that we observed to be expressed in these tissues that fit within the quantitative selection of log 2 or greater difference was ADAMTS 10 which followed the pattern of MMPs 8 and 19.

In order to validate the mRNA expression patterns of the MMPs and ADAMTS that were observed with the transcriptional profiling experiments, quantitative real time RT-PCR analysis was carried out with a subset of the MMPs and ADAMTS that characterize the expression patterns of each cluster. These data are summarized Table 4. As can be seen in the comparison of these data and those presented in Figure 5 and 6, the expression patterns seen from the profiling experiments and those determined by the more accurate RT-PCR technique appear very similar. The one exception was ADAMTS 1 which showed a higher level of expression at day 3 than

in the profiling experiment. These data, in general, validate the observed profiles seen from the clustering data obtained from our transcriptional profiling analysis.

3. Discussion

Studies of developmental, pathological, and pharmacological mechanisms are progressively making use of transcriptional profiling and computational analysis to shed understanding on these processes (Su et al., 2002; Golub et al., 1999; Armstrong et al., 2002). The biological complexity of fracture healing and its defined time frame makes it a particularly excellent biological model to apply transcriptional profiling. Two previous studies have used large scale transcriptional profiling to study rat femur fracture healing. In one study, transcriptional profiling was used to identify how fracture healing might be different in adult and juvenile rats. The comparison of the transcriptional profiles of the two ages of rats, demonstrated that aged rats had quantitatively lower expression for a number of bone matrix mRNAs including osteocalcin and collagen type I. However, this study failed to identify changes in any expressed mRNAs for regulatory factors that controlled the initial healing process such as BMPs or the early cartilage formation during fracture healing was quantitatively or temporally different between the two ages. This lead these authors to conclude that the delayed union in older animals was not due to an altered repair process during the period of cartilage formation, but rather were related to other genes associated with the secondary bone formation and remodeling (Desai et al., 2003).

A different study by Hadjiargyrou et al. (2002) used suppressive subtractive hybridization cloning to generate a cDNA library of those mRNAs that are selectively up-regulated in fracture calluses during the time course of healing. In this study, cluster analysis methods were used to identify groupings of expressed mRNAs that might be of potential functional importance during fracture healing. Although the full complement of genes that were expressed during fracture healing was not assessed, several novel gene families which contribute to fracture healing were identified. It is interesting that using a cluster analysis approach in this study, lead to the discovery of the involvement of the wnt family of morphogenetic factors during fracture healing. This observation is of particular interest given that this family of morphogens has recently been shown to be central regulators of skeletal cell differentiation (Boyden et al., 2002; Bennett et al., 2005; Glass et al., 2005). These two

studies then provide differing examples of how transcriptional profiling might be applied to gain insight into the biological mechanisms that contribute to a complex processes such as fracture healing.

In the study reported here, a genome wide approach was used to examine the expressions patterns of mRNAs for about a third of the known genes in the mouse and a self organizing mapping approach was used to analyze the mRNA expression patterns. One of the unique features of our study was that the cluster analyses were visualized as two dimensional mosaics of colored tiles [data not shown] (Eichler et al., 2003). This type of analysis assigns genes to tiles in a mosaic instead of the more commonly presented colored bars that are used to depict mRNA clusters. In this way, genes that are assigned to a specific area in the mosaic based on their differences in expression relative to unfractured bone, can be easily be related to those assigned in neighboring tiles. Thus, genes having similar temporal and quantitative patterns of expression can be identified in an intuitively obvious and easy to observe. This approach gave us the means of identifying simultaneous gene activities across time without prior assumptions of any structure in the data. As an example, we where able to identify very specific patterns of expression for several of the MMPS and (MMP2/14/Timp2 and MMP9/13) and could show that they appeared to occur in a temporally coordinated manner. Concerning the expression profiles of the ECM protein mRNAs, a diverse set of mRNAs encoding proteins associated with basement membranes, connective tissues of blood vessels, cartilage and type I matrices were all shown to follow a similar temporal profile of induction based upon there positions in the mosaic patterns of mRNA expression. The expression of some of these genes such as collagen types III, IV, VI, XVI, and laminin while all having been examined during normal bone and endochondral development (Durr et al., 1996; Hausler et al., 2002; Kassner et al., 2003; Luther et al., 2003), have not been reported in fracture healing and clearly now merit further examination.

Because the expression of various MMP mRNAs showed such strong statistical correlation as a group or "cluster" that temporally moved together, these preliminary data directed the focus of this study towards defining the temporal relationships between the expression profiles of extracellular matrix proteins and the larger group of proteases and cellular functions that are involved in the remodeling and turnover of the extracellular. Two biological processes of fracture healing that are critical to the progression of the endochondral bone formation and bone repair are tissue vascularization and the resorption of the endochondral tissues (Vu et al., 1998; Gerber et al., 1999; Zhou et al., 2000; Street et al., 2002; Ortega et al., 2003). Previous studies have shown that MMPs carry

out essential roles during both normal skeletal development and during adult fracture repair and are uniquely activated during endochondral development (Colnot et al., 2003; Holmbeck et al., 2003; Ortega et al., 2003; Zhou et al., 2000; Jimenez et al., 2001). A number of other studies have also shown that many of the MMPs are activated during the pathological turnover of cartilage during both rheumatoid and osteo-arthritic processes (Cho et al., 2003; Glasson et al., 2004). While many studies have focused on individual MMPs, only a few have tried to assess how the proteolytic activities of the various MMPs are coordinated. Our studies would suggest that the expression TIMP2/MMP2/ MMP14 and MMP9/MMP13 are two separate groups that are coordinately regulated. In this context several recent studies have shown that MMP14/MT-1, MMP2 and TIMP2 are associated together in a protein complex and that pro MMP2 is only activated in conjunction with MMP14 and TIMP2 (Apte et al., 1997; Jo et al., 2000; Karagiannis and Popel, 2004). Studies of both pathological turnover of articular cartilage, as well as normal developmental remodeling of endochondral cartilage, have shown that MMPs 9 and 13 are also concurrently expressed (Vu et al., 1998; Lehmann et al., 2005; Kevorkian et al., 2004).

Another finding from these results is very suggestive to specific mechanisms by which calcified cartilage is resorbed. These studies showed that very low levels of osteoclasts associated markers were expressed during the first ten days of fracture healing (Rousselle and Heymann, 2002). The observed elevation of two separate antagonists to RANK-L, osteoprotegerin, and TNF super family member 22 was also consistent with this suggestion. TNF super family member 22 is of considerable interest and its expression during cartilage remodeling represents a novel observation, since TNFSF22 is a decoy receptor for TRAIL and can also block the activities of RANK-L. The absence of the expression of mRNAs that are associated with osteoclast function, concurrent with the increased expression of two different antagonist for the key regulator of osteoclast formation (RANK-L) suggest that osteoclast activity only begins after initial periods of fracture healing and cartilage formation. Placing these results in temporal relationship to the expression data for MMP supports the suggestion that the recruitment of osteoclasts into the cartilaginous callus tissue is very tightly controlled and that osteoclast activity only begins after the initiation of the proteolytic activities of the MMPs (Blavier and Delaisse, 1995)

Finally, the observations of the reduction in the expression levels of MMP8 also have potential biological relevance. Since MMP8 is found predominantly in neutrophils, these data would suggest that this cell type is largely absent in the healing tissues, until the marrow element has been reestablished during the late phases of

primary bone formation. MMP8 mRNA has also been shown to be expressed at very low levels during the pathological turnover of cartilage associated with osteoarthritis but is found at higher levels in rheumatoid arthritis suggesting that osteoarthritis has some similarities to a normal endochondral process (Glasson et al., 2004). Investigation of the general role of neutrophils in pathological healing may warrant additional study.

Much less is known concerning the expression and mechanisms of remodeling and resorption of cartilage proteoglycans during endochondral development, although it is now clear that members of the ADAMTS family of proteases appear to be present in cartilage (Kevorkian et al., 2004; Tortorella et al., 1999; Apte, 2004). Several studies have shown that that ADAMTS 4 and 5 are in abundance in both in osteoarthritic cartilage and during endochondral remodeling. On the other hand, transgenic animals with deficiencies in ADAMTS 4 the most prevalent of aggrecanase in cartilage, still appear to undergo both normal development and progressive osteoarthritic degradation under experimental conditions (Glasson et al., 2004; Cal et al., 2002). The studies reported here are the first ones to date that have examined the expression of the ADAMTS gene family during fracture healing and showed like other developmental studies, that ADAMTS 4 is present during endochondral resorption. A second family member ADAMTS 15, followed the expression of ADAMTS 4. ADAMTS 15 based on sequence analysis would also be considered an aggrecanases (Apte, 2004) although its functional role in endochondral resorption is unproven. ADAMTS 1 also has an aggrecanase like sequences but it reached maximal levels of expression later than ADAMTS 4 and 15.

While our initial experiments were very limited relative to the number of time points and the families of gene expression that were examined, this study provided a convincing preliminary set of data related to the complex interplay between the ADAMTS, MMPs and resorptive activities of osteoclasts during extracellular matrix remodeling in a fracture callus. These initial data identified many of the extracellular matrix protein mRNAs that showed the largest quantitative change in their expression during cartilage and bone tissue formation and suggest future lines of study to examine specific interactions between cells types that express various the MMPs or ADAMTS and specific extracellular matrix proteins. Finally these data demonstrate how large-scale transcriptional profiling data is able to uncover numerous complex relationships between various molecular processes that are occurring during fracture healing. Future studies containing additional time points and

comparing transgenic mice with defined deficiencies in a single gene will obtain more exact functional data during fracture healing.

4. Experimental Procedures

4.1. Generation of murine tibia fractures

Research was conducted in conformity with all Federal and USDA guidelines, as well as an IACUC approved protocol. All studies were performed on male 8-10 weeks old C57BL/6J (B6) mice. Age, sex and genetic strain of mouse were based on previous data, in which the time course of fracture healing had been established by both histological and selected candidate gene assessment (Kon et al., 2001; Cho et al., 2002; Gerstenfeld et al., 2003b). A modification of the method of Bonnarens and Einhorn (1984), as previously described (Kon et al., 2001) was used to create simple transverse closed unilateral fractures in the left tibia of all mice. A fracture, whose configuration was inconsistent with standardized placement criteria (mid-diaphyseal) or observed to be grossly comminuted were not used in our studies. Mice were euthanized at selected time points after fracture by CO_2 asphyxiation.

4.2. Time points of analysis

Specific time points over the course of fracture healing were chosen to assess representative periods in the inflammatory phase (day 3); a mid time point in the endochondral phase (day 10); and a period of primary bone formation and coupled remodeling (day 21). The selection of these points was based on empirical knowledge of this model. The more limited number of time points was chosen to simplify the analysis to the three periods when specific biological processes would be at their peak expression.

4.3. RNA preparation

After euthanasia limbs were rapidly disarticulated and surrounding muscular was carefully removed with care being taken to not disrupt the fracture site or callus tissues. Callus tissues were circumscribed by 5 mm on either side of the fracture and an identical site was excised from the mid half of the unfractured contralateral tibiae. The fracture calluses were collected into liquid nitrogen and stored at -80 °C until ready for RNA

extraction. Tissues were powdered under liquid nitrogen and total RNA was extracted by Trizol (Gibco BRL, Gaithersburg, MD, USA) as previously described (Kon et al., 2001). RNAs to be used for microarray were redissolved in Trizol and extracted a second time. After isopropanol precipitation, RNA was dissolved in RNase free water and further purified by using RNeasy mini columns (Qiagen Inc, Valencia, CA). Column preparations were carried out twice according to the manufacturer's instructions. At this point, the RNAs are precipitated with Na Acetate 300mM and 2.5 volumes of 100% EtOH and stored until use.

4.4. Ribonuclease protection assay analysis

For validation of individual genes, ribonuclease protection assays (RPA) were carried out. All template sets were from PharMingen Corp. (San Diego, CA). Assays for bone extracellular matrix genes were carried out with 3µg of total mRNA. Single stranded ^{32}P-labeled cRNA probes and denaturing acrylamide gels analysis were as previously described (Cho et al., 2002). All data sets were normalized to the housekeeping gene L32.

4.5. Reverse transcriptase - PCR

Identical RNA preparations were used for RT-PCR as for the transcriptional expression profiling. All reagents for the PCR analysis were from Applied Biosystems, Inc, and plate assays were read on an ABI 7700 Sequence Detector (Applied Biosystems, Foster City, CA). One µg of total RNA was used for each preparation of cDNA. All cDNA preparations were generated by random hexamer priming. Reverse transcription reactions were initiated at 25° C for 10 minutes and subsequently carried out for an additional 60 minutes at 37° C. The cDNAs were diluted at a ratio of 1:50 in RNase-free water for all PCR reactions. All external and internal primers were from commercial sets available from Applied Biosystems, Inc (Table 1). Each plate contained two negative controls and a positive control probe. The endogenous control (β-actin) was used in all experimental samples for normalization and quantification of each target sequence. All samples were run in triplicates.

The fractional cycle number at which the fluorescence passes the fixed threshold (C_T values) was used for quantification by using a comparative C_T method. This method is described within the Applied Biosystems, Inc instructional manual for the instrumentation. In this method, the threshold (C_T values) is determined when fluorescence of probe reaches its exponential phase of accumulation. Sample values are then normalized to the

threshold value for β-actin (Actb) for each time-point: $\Delta C_T = X\ C_T (exp) - X\ C_T (Actb)$. The C_T value for day 0 was then used as a reference. $\Delta\Delta C_T = X\ C_T (exp) - X\ C_T (exp\ day\ 0)$. The fold change in mRNA expression for each time point was plotted in a graph using day 0 as a reference: $2^{-\Delta\Delta CT(day\ 0)} = 1$.

4.6. Microarray hybridization and image analysis

Slide printing, array labeling, hybridization, and slide reading were performed at the Massachusetts General Hospital Genomics Core Facility. Slides containing the Operon Mus musculus V1.1 probe set (Qiagen) of over 13,000 70-mer oligonucleotide probes were printed by the Massachusetts General Hospital Microarray Core Facility. All slides were quality control tested after printing and contained appropriate positive and negative control sequences for data analysis. RNA from unfractured tibiae was used as the reference. Each experiment contained the reference and a test sample. The Atlas Power script Fluorescent Labeling Kit (Clontech Cat # K1860-1) was used to generate labeled cDNAs. The test and reference RNAs were separately reverse transcribed into amine modified cDNAs using either Cy3 or Cy5 labeling flouros. Slides were hybridized simultaneously with both labeled probes and the data was collected. A GenePix 4000B microarray scanner and software (Axon Instruments) were used to quantify the micro arrays. All data was stored as a ratio of the fluorescent intensity of the reference to the experimental. The BioArray Software Environment (BASE) (Saal et al., 2002) was used for performing the quality control steps in initial filtering the data.

4.7. Data normalization and filtering

The data was normalized by scaling all individual intensities such that the total intensity was the same for both comparative samples (control and fractured) within a single array and across replicate arrays for that time-point. The scaling is important to eliminate variation in effects of differences in fluorescent intensities with different probes. Data from the replicate arrays were then combined to identify outliers and reduce statistical variation in the data. Genes with only one data point after initial selection, due to missing or unreadable data, were excluded. The data was combined using the mean of the replicate ratios.

Using the standard $\log_2$ ratio of the two dye intensities from each array spot representing each gene, the distribution of the log ratios was obtained for both the individual and combined replicates. In general these distributions fall within two SD within the ratio intensities plots and mean ratio and standard deviations are

calculated only from these data. This allows one to identify genes that were expressed sufficiently above the noise without having to resort to an arbitrary minimum ratio value. Genes with low intensities at the level of the background were excluded from the analysis. The data was visualized using log ratio-intensity versus log intensity product on a standard R-I plot, see Figure 2 The plot reveals the intensity-specific artifacts in the $\log_2$ ratio measurements. The one and two standard deviation cutoffs also reveal the inherent "noise level" limitation in the $\log_2$ ratio measurements. We carried out a number of analyses for those genes for which data was available across all time points. Genes that did not change by more than two standard deviations (as defined by the RI plot) in at least one time point were discarded to reduce complexity in later analysis.

4.8 Cluster analysis of normalized data

Once a final data set of high quality probe measurements was attained, we used both hierarchical clustering (Eisen et al., 1998; Tamayo et al., 1999) and a self-organizing maps (SOM) (Kohonen and Somervuo, 2002) based approach to aid in clustering similar behaving genes. Since the results were comparable across both methods, only data from the SOM analysis is included in this report. The SOM analysis was performed using the Gene Expression Dynamics Inspector (GEDI) software package that displays high-dimensional gene expression profiles as colored coded mosaic images (Eichler et al., 2003). Based on position of a genes placement within a given tile within the mosaic, the patterns of gene expression may be easily identified without any prior assumptions about the gene's expression. A genes placement within a tile is based on its quantitative level of expression and tiles within proximity to other tiles in the mosaic have similar quantitative levels of expression.

Acknowledgements

The authors would like to acknowledge that this work has been supported by a contract from the DOD DAMD17-03-0576 (LCG). Institutional support was provided by the Department of Orthopedic Surgery at the Boston University School of Medicine (TAE). Portions of this study are derived from the thesis of KW presented in partial fulfillment of his requirements for the Master of Medical Sciences. CE was supported on NIH grant NIAMS AR 47045 (LCG).

References

Apte, S.S., 2004. A disintegrin-like and metalloprotease (reprolysin type) with thrombospondin type1 motifs: ADAMTS family. Intl. J. Biochem. Cell. Biol. 36, 981-985.

Apte, S.S., Fukai, N., Beier, D.R., Olsen, B.R., 1997. The matrix metalloproteinase-14 (MMP-14) gene is structurally distinct from other MMP genes and is co-expressed with the TIMP-2 gene during mouse embryogenesis. J. Biol. Chem. 272, 25511-25517.

Armstrong, S.A., Staunton, J.E., Silverman, L.B., Pieters, R., den Boer, M.L., Minden, M.D., Sallan, S.E., Lander, E.S., Golub, T.R., Korsmeyer, S.J., 2002. MLL translocations specify a distinct gene expression profile that distinguishes a unique leukemia. Nat. Genet. 30, 41-47.

Balint, E., Lapointe, D., Drissi, H., van der Meijden, C., Young, D.W., van Wijnen, A.J., Stein, J.L., Stein, G.S., Lian, J.B., 2003. Phenotype discovery by gene expression profiling: mapping of biological processes linked to BMP-2-mediated osteoblast differentiation. J. Cell. Biochem. 89, 401-426.

Barnes, G.L., Della Torre, T., Sommer, B., Young, M.F., Gerstenfeld, L.C., 2002. Transcriptional regulation restricting bone sialoprotein gene expression to both hypertrophic chondrocytes and osteoblasts. Cell. Biochem. 87; 458-469.

Barnes, G.L., Kostenuik, P.J., Gerstenfeld, L.C., Einhorn, T.A., 1999. Growth factor regulation of fracture repair. J. Bone. Miner. Res. 14, 1805-1815.

Bennett, C.N., Longo, K.A., Wright, W.S., Suva, L.J., Lane, T.F., Hankenson, K.D., MacDougald, O.A., 2005. Regulation of osteoblastogenesis and bone mass by Wnt10b. Proc Natl Acad Sci USA. 102, 3324-3329.

Blavier, L., Delaisse, J.M., 1995. Matrix metalloproteinases are obligatory for the migration of preosteoclasts to the developing marrow cavity of primitive long bones. J. Cell. Sci. 108, 3649-3659.

Bolander, M.E., 1992. Regulation of fracture repair by growth factors. Proc. Soc. Exp. Biol. Med. 200, 165-170.

Bonnarens, F., Einhorn, T.A., 1984. Production of a standard closed fracture in laboratory animal bone. J. Orthop. Res. 2, 97-101.

Boyden, L.M., Mao, J., Belsky, J., Mitzner, L., Farhi, A., Mitnick, M.A., Wu, D., Insogna, K., Lifton, R.P., 2002. High bone density due to a mutation in LDL-receptor-related protein 5. N Engl J Med. 346, 1513-1521.

Cal, S., Obaya, A.J., Llamazares, M., Garabaya, C., Quesada, V., Lopez-Otin, C., 2002. Cloning, expression analysis, and structural characterization of seven novel human ADAMTS, a family of metalloproteinases with disintegrin and thrombospondin-1 domains. Gene. 283, 49-62.

Cho, T.J., Gerstenfeld, L.C., Einhorn, T.A., 2002. Differential temporal expression of members of the transforming growth factor beta superfamily during murine fracture healing. J. Bone. Miner. Res. 17, 513-520.

Cho, T.J., Lehmann, W., Edgar, C., Sadeghi, C., Hou, A., Einhorn, T.A., Gerstenfeld, L.C., 2003. Tumor necrosis factor alpha activation of the apoptotic cascade in murine articular chondrocytes is associated with the induction of metalloproteinases and specific pro-resorptive factors. Arthritis. Rheum. 48, 2845-2854.

Colnot, C., Thompson, Z., Miclau, T., Werb, Z., Helms, J.A., 2003. Altered fracture repair in the absence of MMP9. Development. 130, 4123-4133.

Desai, B.J., Meyer, M.H., Porter, S., Kellam, J.F., Meyer, R.A. Jr., 2003. The effect of age on gene expression in adult and juvenile rats following femoral fracture. J. Orthop. Trauma. 17, 689-698.

Durr, J., Lammi, P., Goodman, S.L., Aigner, T., von der Mark, K., 1996. Identification and immunolocalization of laminin in cartilage. Exp. Cell. Res. 222, 225-233.

Eichler, G.S., Huang, S., Ingber, D.E., 2003. Gene Expression Dynamics Inspector (GEDI): for integrative analysis of expression profiles. Bioinformatics. 19, 2321-2322.

Eisen, M.B., Spellman, P.T., Brown, P.O., Botstein, D., 1998. Cluster analysis and display of genome-wide expression patterns. Proc. Natl. Acad. Sci. USA. 95, 14863-14868.

Ferguson, C., Alpern, E., Miclau, T., Helms, J.A., 1999. Does adult fracture repair recapitulate embryonic skeletal formation? Mech. Dev. 87, 57-66.

Gerber, H.P., Vu, T.H., Ryan, A.M., Kowalski, J., Werb, Z., Ferrara, N., 1999. VEGF couples hypertrophic cartilage remodeling, ossification and angiogenesis during endochondral bone formation. Nat. Med. 5, 623-628.

Gerstenfeld, L.C., Cho, T.J., Kon, T., Aizawa, T., Tsay, A., Fitch, J., Barnes, G.L., Graves, D.T., Einhorn, T.A., 2003a. Impaired fracture healing in the absence of TNF-alpha signaling: the role of TNF-alpha in endochondral cartilage resorption. J Bone Miner Res. 18, 1584-1592.

Gerstenfeld, L.C., Cullinane, D.M., Barnes, G.L., Graves, D.T., Einhorn, T.A., 2003b. Fracture healing as a post-natal developmental process: molecular, spatial, and temporal aspects of its regulation. J. Cell. Biochem. 88, 873-884.

Glass, D.A. 2nd, Bialek, P., Ahn, J.D., Starbuck, M., Patel, M.S., Clevers, H., Taketo, M.M., Long, F., McMahon, A.P., Lang, R.A., Karsenty, G, 2005. Canonical Wnt signaling in differentiated osteoblasts controls osteoclast differentiation. Dev Cell. 8, 751-764.

Glasson, S.S., Askew, R., Sheppard, B., Carito, B.A., Blanchet, T., Ma, H.L., Flannery, C.R., Kanki, K., Wang, E., Peluso, D., Yang, Z., Majumdar, M.K., Morris, E.A., 2004. Characterization of and osteoarthritis susceptibility in ADAMTS-4-knockout mice. Arthritis. Rheum. 50, 2547-2558.

Golub, T.R., Slonim, D.K., Tamayo, P., Huard, C., Gaasenbeek, M., Mesirov, J.P., Coller, H., Loh, M.L., Downing, J.R., Caligiuri, M.A., Bloomfield, C.D., Lander, E.S., 1999. Molecular classification of cancer: class discovery and class prediction by gene expression monitoring. Science. 286, 531-537.

Hadjiargyrou, M., Lombardo, F., Zhao, S., Ahrens, W., Joo, J., Ahn, H., Jurman, M., White, D.W., Rubin, C.T., 2002. Transcriptional profiling of bone regeneration: Insight into the molecular complexity of wound repair. J. Biol. Chem. 277, 30177-30182.

Hausler, G., Helmreich, M., Marlovits, S., Egerbacher, M., 2002. Integrins and extracellular matrix proteins in the human childhood and adolescent growth plate. Calcif. Tissue. Int. 71, 212-218.

Holmbeck, K., Bianco, P., Chrysovergis, K., Yamada, S., Birkedal-Hansen, H., 2003. MT1-MMP-dependent, apoptotic remodeling of unmineralized cartilage: a critical process in skeletal growth. J. Cell. Biol. 163, 661-671.

Jimenez, M.J., Balbin, M., Alvarez, J., Komori, T., Bianco, P., Holmbeck, K., Birkedal-Hansen, H., Lopez, J.M., Lopez-Otin, C., 2001. A regulatory cascade involving retinoic acid, Cbfa1, and matrix metalloproteinases is coupled to the development of a process of perichondrial invasion and osteogenic differentiation during bone formation. J. Cell. Biol. 155, 1333-1344.

Jo, Y., Yeon, J., Kim, H.J., Lee, S.T., 2000. Analysis of tissue inhibitor of metalloproteinases-2 effect on pro-matrix metalloproteinase-2 activation by membrane-type 1 matrix metalloproteinase using baculovirus/insect-cell expression system. Biochem. J. 345, 511-519.

Karagiannis, E.D., Popel, A.S., 2004. A Theoretical Model of Type I Collagen Proteolysis by Matrix Metalloproteinase (MMP) 2 and Membrane Type 1 MMP in the Presence of Tissue Inhibitor of Metalloproteinase 2. J. Biol. Chem. 279, 39105-39114.

Kassner, A., Hansen, U., Miosge, N., Reinhardt, D.P., Aigner, T., Bruckner-Tuderman, L., Bruckner, P., Grassel, S., 2003. Discrete integration of collagen XVI into tissue-specific collagen fibrils or beaded microfibrils. Matrix. Biol. 22, 131-143.

Kevorkian, L., Young, D.A., Darrah, C., Donell, S.T., Shepstone, L., Porter, S., Brockbank, S.M., Edwards, D.R., Parker, A.E., Clark, I.M., 2004. Expression profiling of metalloproteinases and their inhibitors in cartilage. Arthritis. Rheum. 50, 131-141.

Kohonen, T., Somervuo, P., 2002. How to make large self-organizing maps for nonvectorial data. Neural. Netw. 15, 945-952.

Kon, T., Cho, T.J., Aizawa, T., Yamazaki, M., Nooh, N., Graves, D., Gerstenfeld, L.C., Einhorn, T.A., 2001. Expression of osteoprotegerin, receptor activator of NF-kappaB ligand (osteoprotegerin ligand) and related proinflammatory cytokines during fracture healing. J. Bone. Miner. Res. 16, 1004-10014.

Lehmann, W., Edgar, C.M., Wang, K., Cho, T.J., Barnes, G.L., Kakar, S., Graves, D.T., Rueger, J.M., Gerstenfeld, L.C., Einhorn, T.A., 2005. Tumor necrosis factor alpha (TNF-alpha) coordinately regulates the expression of specific matrix metalloproteinases (MMPS) and angiogenic factors during fracture healing. Bone. 36, 300-310.

Luther, F., Saino, H., Carter, D.H., Aaron, J.E., 2003. Evidence for an extensive collagen type III/VI in the proximal domain of rat femur. I. Diminution with ovariectomy. Bone. 32, 652-659.

Ortega., N., Behonick, D., Stickens, D., Werb, Z., 2003. How proteases regulate bone morphogenesis. Ann. NY. Acad. Sci. 995,109-116.

Rousselle, A.V., Heymann, D., 2002. Osteoclastic acidification pathways during bone resorption. Bone. 30, 533-540.

Saal, L.H., Troein, C., Vallon-Christersson, J., Gruvberger, S., Borg, A., Peterson, C., 2002. BioArray Software Environment (BASE): a platform for comprehensive management and analysis of microarray data. Genome. Biology. 3, software0003.0.

Street, J., Bao, M., deGuzman, L,, Bunting, S., Peale, F.V. Jr., Ferrara, N., Steinmetz, H., Hoeffel, J., Cleland, J.L., Daugherty, A., van Bruggen, N., Redmond, H.P., Carano, R.A., Filvaroff, E.H., 2002. Vascular endothelial growth factor stimulates bone repair by promoting angiogenesis and bone turnover. Proc. Natl. Acad. Sci. USA. 99, 9656-9661.

Stock, M., Schafer, H., Fliegauf, M., Otto, F.J., 2004. Identification of novel genes of the bone-specific transcription factor Runx2. J. Bone. Miner. Res. 19, 959-972.

Su, A.I., Cooke, M.P., Ching, K.A., Hakak, Y., Walker, J.R., Wiltshire, T., Orth, A.P., Vega, R.G., Sapinoso, L.M., Moqrich, A., Patapoutian, A., Hampton, G.M., Schultz, P.G., Hogenesch, J.B., 2002. Large-scale analysis of the human and mouse transcriptomes. Proc. Natl. Acad. Sci. USA. 99, 4465-4470.

Tamayo, P., Slonim, D., Mesirov, J., Zhu, Q., Kitareewan, S., Dmitrovsky, E., Lander, E.S., Golub, T.R., 1999. Interpreting patterns of gene expression with self-organizing maps: methods and application to hematopoietic differentiation. Proc. Natl. Acad. Sci. USA. 96, 2907-2912.

Tortorella, M.D., Burn, T.C., Pratta, M.A., Abbaszade, I., Hollis, J.M., Liu, R., Rosenfeld, S.A., Copeland, R.A., Decicco, C.P., Wynn, R., Rockwell, A., Yang, F., Duke, J.L., Solomon, K., George, H., Bruckner, R., Nagase, H., Itoh, Y., Ellis, D.M., Ross, H., Wiswall, B.H., Murphy, K., Hillman, M.C. Jr., Hollis, G.F., Newton, R.C., Magolda, R.L., Trzaskkos, J.M., Arner, E.C., 1999. Purification and cloning of aggrecanase-1: a member of the ADAMTS family of proteins. Science. 284, 1664-1666.

Vortkamp, A., Pathi, S., Peretti, G.M., Caruso, E.M., Zaleske, D.J., Tabin, C.J., 1998. Recapitulation of signals regulating embryonic bone formation during postnatal growth and in fracture repair. Mech. Dev. 71, 65-76.

Vu, T.H., Shipley, J.M., Bergers, G., Berger, J.E., Helms, J.A., Hanahan, D., Shapiro, S.D., Senior, R.M., Werb, Z., 1998. MMP-9/gelatinase B is a key regulator of growth plate angiogenesis and apoptosis of hypertrophic chondrocytes. Cell. 93, 411-422.

Zhou, Z., Apte, S.S., Soininen, R., Cao, R., Baaklini, G.Y., Rauser, R.W., Wang, J., Cao, Y., Tryggvason, K., 2000. Impaired endochondral ossification and angiogenesis in mice deficient in membrane-type matrix metalloproteinase I. Proc. Natl. Acad. Sci. USA. 97, 4052-4057.

Figure Legends

Figure 1. RNA expression analysis of selected extracellualr matrix protein mRNAs across the time course of fracture healing by RPA. **Panel A)** Representative autoradiographic images of the RPA products as resolved on a 6% PAGE sequencing gel. Days after fracture and positions of each protected species are denoted. **Panel B)** The graphic analysis of the relative mRNA levels of selected genes. Radioactive counts of the protected bands were determined by direct β– counting on a flat surface beta detector. Band counts were normalized to the ratio of the internal standard, L32, and expressed as a relative value.

Figure 2. A representative example of the spot analysis from one replicate for osteocalcin expression is presented. The assay samples are denoted in lane one. The raw fluorescent intensities that were obtained with the reciprocal Cy3/Cy5 cDNA labeling and hybridization are shown in channels one and two. The upper and lower halves of the read out show the two data sets from reversing Cy3/Cy5 hybridizations between the experimental and reference samples. The ratio of reference channel to the experimental channel is shown in the third lane. The descriptive visual presentation of the log variation form reference is presented descriptively as green (low) or red (high). The spot size and observed spots images are shown in the last two lanes.

Figure 3. Ratio Intensity plots of total numbers of expressed mRNAs at various times after fracture. RI plots were generated as a visual representation of uniquely overexpressed and underexpressed genes. We used unfractured bone (day 0) as our reference and saw the greatest variance in uniquely expressed genes showing log 2 fold greater or lesser from the reference in the day 3 and day 10 samples in comparison to the day 21 sample. The numbers of observed spots that fall within two standard deviations of conformity of normalized spot intensity are shown with dotted lines 1SD standard and with a dashed line 2SD.

Figure 4. Graphical Presentation of Various SOMs patterns for the MMPs and TIMPs. Four separate panels showing the temporal patterns of expression of MMP2/MMP14, MMP9/MMP13, MMP8/MMP19 and TIMPs 1,2,and 3 are shown. Ratio log2 fold change in expression relative to unfractured bone versus time after fracture is presented. The groupings of individual MMPS are denoted within the keys contained in each of the figures.

Figure 5. Graphical Presentation of Various SOMs patterns for the ADAMTs. Three separate panels showing the temporal patterns of expression of ADAMTS 1/10 and ADAMTS 4 /15 are shown. Ratio log2 fold change in expression relative to unfractured bone versus time after fracture is presented. The groupings of individual ADAMTS are denoted within the keys contained in each of the figures.

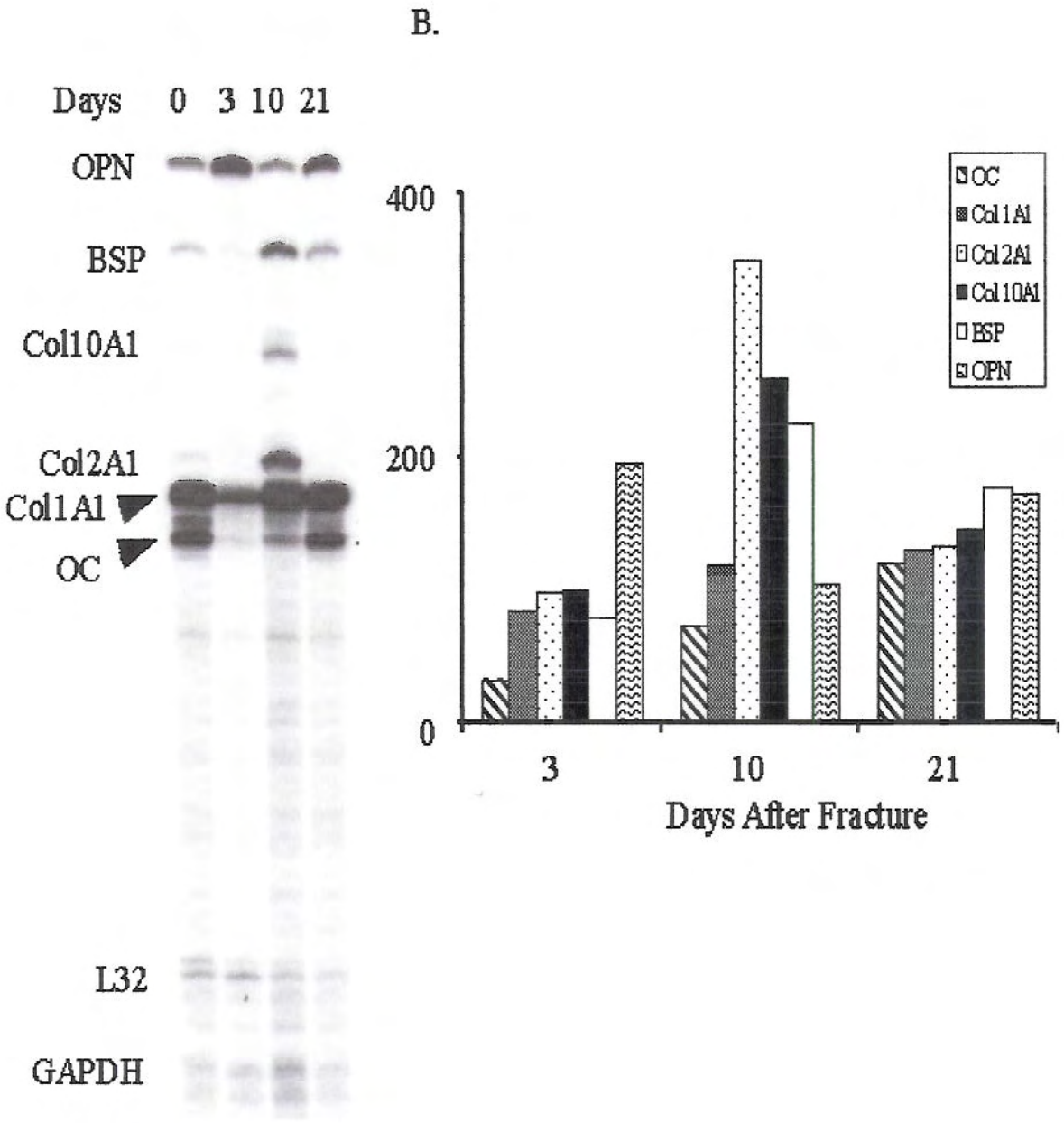
A.
B.
Days 0 3 10 21
OPN
BSP
Col10A1
Col2A1
Col1A1
OC
L32
GAPDH
400
200
0
3
10
21
Days After Fracture
OC
Col1A1
Col2A1
Col10A1
BSP
OPN

Figure 1.

Assay	Ch1 int	Ch2 int	Ratio	log2	Spot size
Day 0	401	23409	0.02	-5.87	
Day 3	597	11177	0.05	-4.23	
Day 10	1276	63133	0.02	-5.63	
Day 21	34136	350	97.53	6.61	
Day 0	553	41015	0.01	-6.21	
Day 3	884	23480	0.04	-4.73	
Day 10	1840	64884	0.03	-5.14	
Day 21	64590	447	144.50	7.17	

Figure 2.

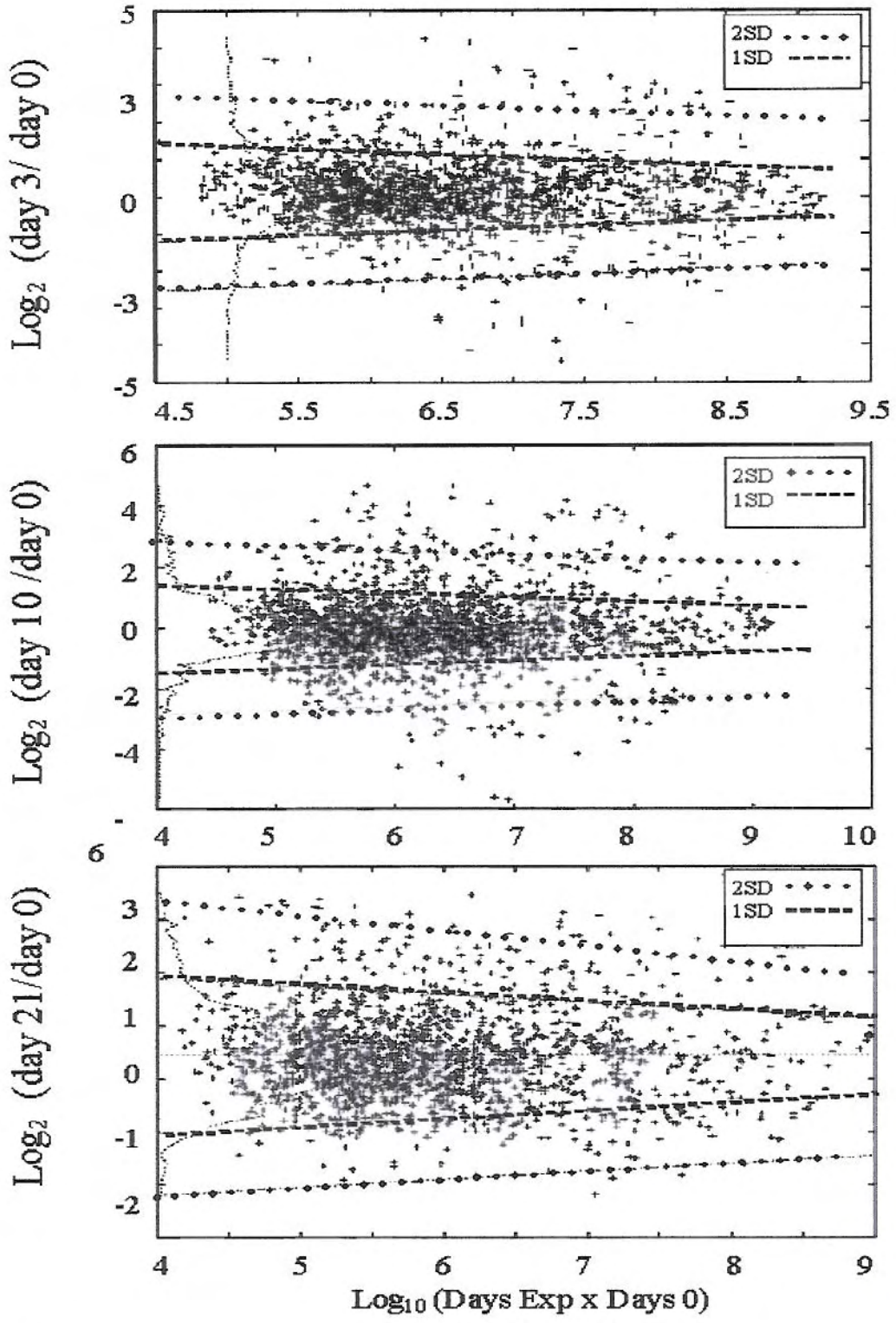
2SD
1SD
Log2 (day 3/ day 0)
Log2 (day 10 /day 0)
Log2 (day 21/day 0)
Log10 (Days Exp x Days 0)

Figure 3.

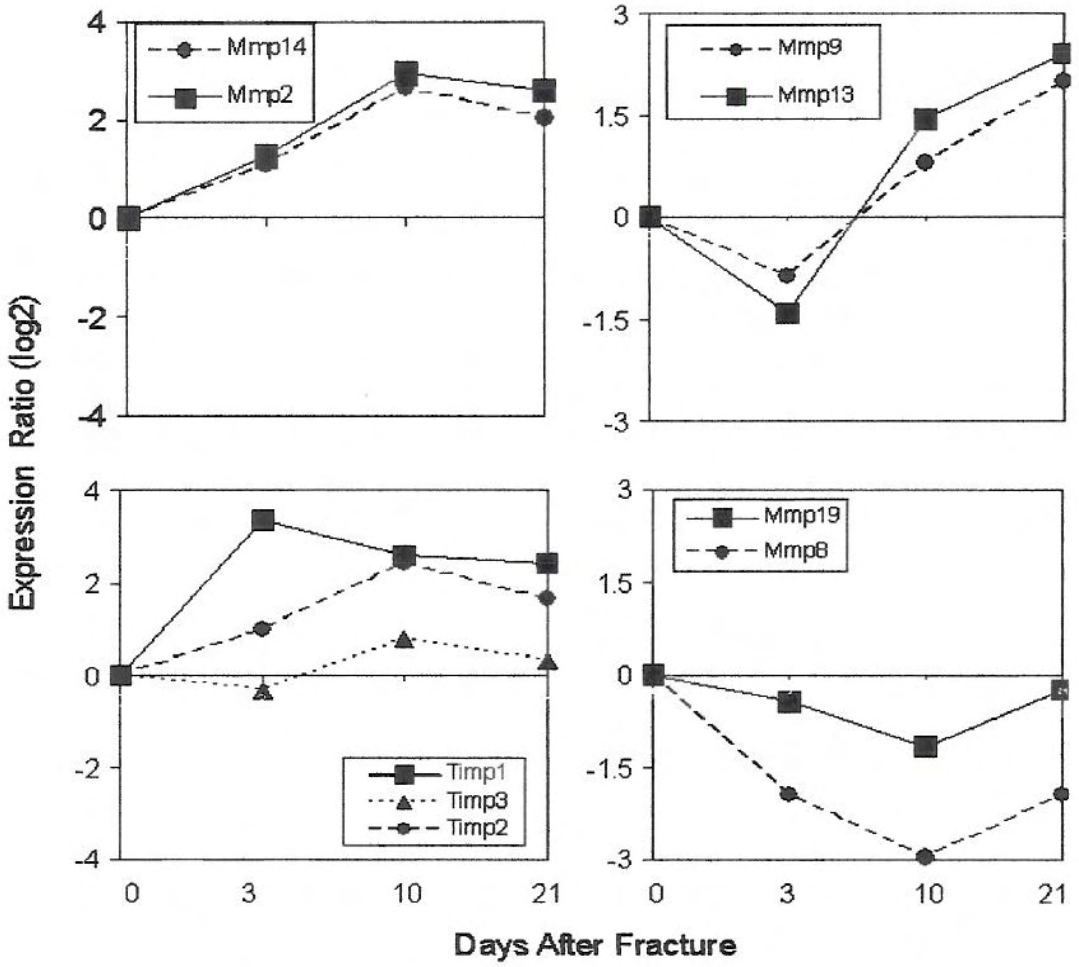
Mmp14
Mmp2
Mmp9
Mmp13
Mmp19
Mmp8
Timp1
Timp3
Timp2
Expression Ratio (log2)
Days After Fracture
4
2
0
-2
-4
3
1.5
0
-1.5
-3
0
3
10
21

Figure 4.

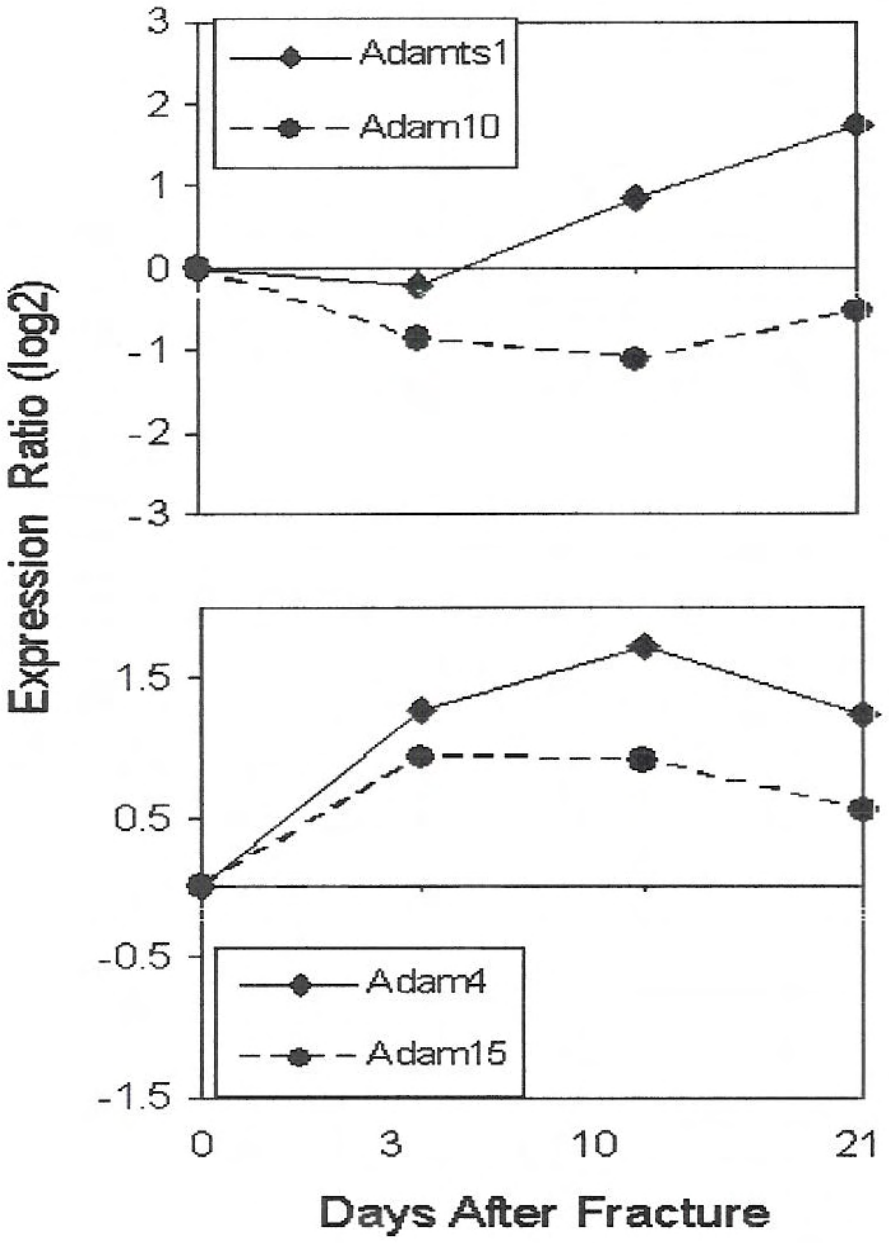
Adamts1
Adam10
Adam4
Adam15
Expression Ratio (log2)
Days After Fracture
3
2
1
0
-1
-2
-3
1.5
0.5
-0.5
-1.5
0
3
10
21

Figure 5.

Table 1. RT-PCR Primers

Gene	UniGene +	Reference Number	Primer Sequence
β-Actin	Mm.297	NM_007393	TACTGAGCTGCGTTTTACACCCTTT
MMP2	Mm.29564	NM_008610	GGACCTGCAGGGCGGTGGTCATAGC
MMP14	Mm.280175	NM_008608	CAGCCCCGAAGCCTGGCTGCAGCAG
MMP13	Mm.5022	NM_008607	AGTTCCAAAGGCTACAACTTGTTTA
MMP8	Mm.16415	NM_008611	AAAAACTGCTGAGAATTACCTACGA
MMP9	Mm.4406	NM_013599	GCATCCAGTATCTGTATGGTCGTGG
Adamts_1	Mm.1421	NM_009621	GGGAAAGCCATCAGGACCAGGAAGC
Adamts_4	Mm.23156	NM_172845	GGACAATGGTTATGGGCACTGCCTC
Adamts_5	Mm.112933	NM_011782	AAAATATTACTCGACATCAAGCCAT

+The unigene, reference number and reverse primer sequence of genes. The forward primer and internal primer that are labeled with FAM sequence are proprietary.

Table 2. Selective Expression Data From Micro-Array Data

Numeric data is the Log 2 value of expression relative to the reference (Un-fractured bone)*

Log 2	Over Expressed	Log 2	Under Expressed
DAY 3			
3.35	fatty acid binding protein 5, Fabp5	-2.16	bone gamma-carboxyglutamate protein, Osteocalcin
3.02	follistatin-like Fst1	-2.18	acid phosphatase 5, tartrate resistant Acp5 hydrolase
2.72	osteoblast specific factor 2 (fasciclin I-like) OSF-2	-3.30	TATA box binding protein
2.45	TNF receptor superfamily member 22	-4.44	carbonic anhydrase 2 Car2 lyase
0.52	TNF receptor superfamily, member 11b (OPG)		
DAY 10			
4.17	cartilage oligomeric matrix protein (Comp)	-2.70	FGF inducible 16 Fin 16
4.05	osteoglycin Ogn	-2.72	high mobility group box 2 Hmgb2
3.82	matrix gamma-carboxyglutamate (gla) protein	-5.69	carbonic anhydrase 2 Car2 lyase
3.7	follistatin-like Fstl heparin binding		
2.98	perlecan (heparan sulfate proteoglycan 2) Hspg2		
2.79	midkine Mdk growth factor; heparin binding		
2.65	insulin-like growth factor binding protein 5 Igfbp5		
1.63	TNF receptor family superfamily member 22		
0.79	TNF receptor superfamily, member 11b (OPG)		
DAY 21			
2.26	twist gene homolog Twist DNA binding; protein	-2.62	neutrophilic granule protein Ngp
2.25	osteoglycin Ogn	-3.18	eosinophil-associated ribonuclease 3 Ear3
1.02	TNF receptor family superfamily member 22		
0.52	TNF receptor superfamily, member 11b (OPG)		

*All values represent the individual mRNAs expression as a ratio between unfractured bone (reference) and the experimental sample. All values are also presented as the log 2 of the value. As an example COMP is expressed as 4.17 log2 fold greater at day ten or ~21 fold higher in expression than unfractured bone. If the mRNA is under expressed the numerical value is log2 fold less than unfractured bone and is expressed as a negative value.

Table 3. Prevalent GEDI Groupings Showing Elevated Expression Throughout The Repair Period

A. Group I

Generalized ECM Proteins
Procollagen type V alpha 1
Procollagen type V alpha 3
Procollagen type VI alpha 2
Procollagen type VI alpha 1
Procollagen type VI, alpha 3
Procollagen type XI, alpha 1
Procollagen type XVI, alpha 11
Procollagen-C endopeptidase enhancer
Collagen triple helix containing 1
Procollagen-Lysine 2-Oxoglutarate 5-Dioxygenase
Osteoglycin

Cartilage Associated
Cartilage oligomeric matrix protein
Perlecan
procollagen gene (IX) alpha2
procollagen type (IX) alpha 1
Ecm1 : Extracellular matrix protein 1

Non Defined Families
Osteoblast specific factor 2
S100 Calcium binding protein
Cadherin 4
Vimentin
Annexin A6

B. Group II
Procollagen type 1 alpha 1
Procollagen type I, alpha 2
Procollagen, type V, alpha 2
Procollagen C-proteinase enhancer protein

Vessel and Basement Membrane Related
Procollagen type IV alpha 1
Procollagen type IV, alpha 2
Thrombospondin 4
Thrombospondin 2
Thrombospondin 1
Laminin beta 2
Laminin gamma 1
Lamin A
Nidogen 1
Procollagen type III alpha1
Fibrillin

TNF Family
TNF receptor superfamily member 22 (TRAIL Decoy)
TNF receptor superfamily, member 11b
(osteoprotegerin)

Table 4. RT-PCR Fold Induction Over Time

Δ Time	Gene							
	MMP2	MMP8	MMP9	MMP13	MMP14	Adamts1	Adamts4	Adamts5
DAY 0	1	1	1	1	1	1	1	1
DAY 3	8.397 +	0.1	0.2	0.3	6.06	5.76	15.24	3.6
DAY 10	19.159	0.3	4.25	10.1	10.126	7.889	19.42	3.45
DAY 21	5.098	0.645	4.8	7.315	4.99	5.57	7.67	3.317

+The fold change in mRNA as normalized to β–actin and expressed as a fold change relative to unfractured bone

Appendix 6

THREE DIMENSIONAL RECONSTRUCTION OF FRACTURE CALLUS MORPHOGENESIS DEMONSTRATE ASYMMETRY IN CALLUS DEVELOPMENT

Louis C. Gerstenfeld[1*], Yaser M. Alkhiary[1, 2], Elizabeth A. Krall[3], Fred H. Nicholls[1], Stephanie N. Stapelton[1], Jennifer L. Fitch[1], Alfie W. Tsay[1], Dana T. Graves[4], Karl J. Jepsen[5], and Thomas A. Einhorn[1]

[1]Orthopaedic Research Laboratory, Boston University Medical Center, Boston, MA

[2]Department of Restorative Sciences/Biomaterials, Boston University School of Dental Medicine, Boston, MA

[3]Department of Health Policy and Health Services Research, Boston University School of Dental Medicine, Boston, MA

[4]Department of Periodontology and Oral Biology, Boston University School of Dental Medicine, Boston, MA

[5]Department of Orthopaedics, Mount Sinai School of Medicine, New York, NY

Running Title: Three Dimensional Histomorphometric Reconstruction of Fractures Calluses

This work was supported by the following grants: NIAMS AR047045 (LCG), NIAMS AR0409920 (TAE), and Department of Defense DAMD17-03-1-0576 (LCG). Institutional support was provided by the Department of Orthopaedic Surgery, Boston University School of Medicine. Portions of this article are derived from the thesis of YA that was submitted in partial fulfillment of his requirement for DSD degree in the Department of Periodontology and Oral Biology, Boston University School of Dental Medicine.

*Corresponding author:

Louis C. Gerstenfeld, Ph.D.

Orthopaedic Research Laboratory

Boston University Medical Center

715 Albany Street, R-205, Boston, MA 02118

Phone: 617-414-1660 Fax: 617-414-1661

lgersten@bu.edu

Author Email Addresses: lgersten@bu.edu; yaser@alkhiary.net; kralle@bu.edu; podded@hotmail.com; snstaple@bu.edu; jenfitch@bu.edu; alfie_t@hotmail.com; dgraves@bu.edu; karl.jepsen@mssm.edu; thomas.einhorn@bmc.org

MICROABSTRACT: The spatial temporal cellular activities of fracture callus morphogenesis were defined using serial sections, standard histological measurements, in situ hybridization and three dimensional tissue reconstruction. These data showed that endochondral bone formation occurred in an asymmetric manner within femur fracture calluses such that cartilage tissues formed predominantly distal and lateral to the fracture and that the spatial confines of the cartilage formation established the spatial patterns of each of the subsequent stages of bone healing.

Introduction: Tissue morphogenesis is controlled by spatial temporal relationships between various cells types and their secreted morphogens. Within a growth plate the spatial arrangements between the various cell types that contribute to the skeletal morphogenesis are defined in large part by the tissue's linear pattern of growth. While fracture repair recapitulates many aspects of endochondral bone formation the morphogenetic pattern of the various tissues that contribute to a fracture healing are not as easily discernable.

Methods: Serial histological sections of mouse and rat fracture calluses were used to define the spatial and temporal changes in tissue composition associated with the progression of fracture healing. In situ hybridization to col1a1 and col2a1 mRNAs were used to define areas of new cartilage and bone formation. Two dimensional representations of tissue composition were compared to three dimensional computer assisted reconstructions using the same serial sections. Reconstructed volumes were used to define the spatial development of the morphogenetic fields that gave rise to the fracture callus.

Results: Both compositional and three dimensional reconstructions demonstrated that cartilage tissue developed, in an asymmetrical pattern around the fracture. After 14 days of fracture healing, approximately 70% of the volume of callus that formed in a mid-diaphyseal femoral fracture was on the distal, lateral aspect of the bone. As the callus developed proximally, the cartilage tissue rotated toward the medial bone surface. Subsequently as fracture healing progressed, trabecular bone replaced the calcified cartilage proceeding from the edges of the callus inward towards the fracture with the area around the fracture to be the last to be replaced. The asymmetric pattern of endochondral bone formation was confirmed by reconstructing the three dimensional pattern of collagen type I (col1a1) and II (col2A1) mRNA expression, as determined by in situ hybridization in mouse femur fractures. These results corroborated those in the rat showing the same asymmetric pattern of

endochondral bone formation. Three dimensional reconstruction of the calluses subsequent to the resorption of the cartilage showed a complex structure in which thin shell of new exterior cortical bone was now supported by an interior structure of trabecular bone that had replaced the original cartilage tissues.

Conclusions: These results demonstrate that specific developmental mechanisms control the asymmetric pattern of callus formation and suggest that this pattern recapitulates the original asymmetry of endochondral tissue development of the femur. On the other hand the spatially coupled mechanisms that remodel the callus from a greater cross sectional diameter to a lesser diameter must be different from the developmental mechanisms that are observed during appositional bone growth.

KEY WORDS:

Orthopaedics, Fracture Repair, Bone Histomorphometry, Growth and Development

INTRODUCTION

Bone is one of the few tissues in the body that undergoes true regeneration in response to injury and many of the mechanisms involved in skeletal repair appear to recapitulate the events of embryologic developmental. [1,2,3] Our present understanding of the basic mechanisms of skeletal repair suggests that it is a multifaceted process involving complex interactions between the immune, hematopoietic, and vascular systems.[4,5,6,7,8] These systems all interact with the underlying mesenchymal cell population within and surrounding bone and contribute to the induction, growth, and/or maintenance of the skeletagenic cellular responses that regenerate the injured tissue. The overall spatial relationships between the morphogenetic fields and the various proximate tissues that contribute to the repair process define the final tissue geometry and composition of the fracture callus. The end result of these developmental processes is the reestablishment of both the original geometry and biomechanical competency of the skeleton.

Because the size, shape and material properties of adult bones are determined early in life and are in part controlled by intrinsic genetic factors,[9,10,11] it is important to understand the biological processes (or factors) that contribute to the variation in these morphometric and material traits. This can be accomplished in the context of the developmental processes that are activated during fracture repair. A quantitative definition of the spatial geometry and nature of the tissue formation (endochondral versus osseous) as well as a definition of the spatial nature of tissue remodeling that regenerates the original bone is also necessary for our understanding of fracture healing. In this study, we conducted a histomorphometric analysis of the temporal progression of fracture healing. We defined tissue compositional measurements, the statistical accuracy of these measurements, and made comparisons of these measurements to three dimensional histological reconstruction of fracture callus tissues at various developmental stages during fracture healing.

In order to link histologic changes with the expression of matrix genes critical to the repair process, the temporal and spatial expression of collagen types I and II mRNAs were assessed by in situ hybridization. The results provide the basic analytical bridge between the cellular and molecular processes that form and maintain skeletal tissues and the geometric and material nature of the callus tissue that produces its mechanical properties. The data further demonstrate that the spatial arrangement of various tissues within the callus develop and heal in

an asymmetric pattern. This asymmetry is suggestive of the original spatial pattern of growth in the uninjured long bone and may correlate with the activity of the proximal or distal physes.

MATERIALS AND METHODS

Production of Simple Transverse Fractures

Animal research was conducted in conformity with all federal and USDA guidelines, as well as an IACUC approved protocol. Male Sprague-Dawley rats (n = 3 per group) weighing 449±39g and about 7-9 months old were used. In experiments assessing mice, male C57BL/6J mice (n = 5 per group) at 8 to 10 weeks of age were used. All rats were purchased from Harlan Bioproducts for Science, Indianapolis, IN and all mice were purchased from Jackson Laboratories, Bar Harbor ME. Closed, simple, mid-diaphyseal, transverse fractures of the rat femurs were produced as described by Bonnarens and Einhorn.[12] A modification of this procedure was used for the mice[5]. However unlike our previous studies in mice in which the tibia was fractured, the femur was fractured in the current studies. In the case of the mouse femur fractures, intramedullary pins were inserted retrograde through the distal condyle of the femur and stabilized in the major trochanter. Radiographic assessment of the fractures was performed immediately after fracture and at the time of euthanasia. Fractures which did not occur in the mid-diaphysis or were excessively comminuted were not used in the study. All animals were euthanized by CO_2 asphyxiation at 7, 14, 21 and 35 days post-fracture. At the time of euthanasia, fracture callus specimens were harvested and carefully cleaned of muscle and soft connective tissue. Callus dimensions were measured at this time in anterior-posterior (AP) and medial-lateral (ML) dimensions using an electronic caliper (# R163-7251006C, Maryland and Metrics, Baltimore, MD).

Tissue Fixation and Decalcification

For histological assessments, the bones with a small amount of surrounding muscle and soft tissues were fixed for 2 days in 4% paraformaldehyde in phosphate buffered saline at 4°C. Specimens were completely decalcified in 14% w/v EDTA changed three times per week for approximately 2-3 weeks while shaking at 4°C. Specimens were rinsed and placed in ice cold PBS for final processing. After decalcification, the intramedullary

pin was removed and the anatomic center of the callus was determined from the x-ray measurements and was set as the point of the transverse fracture. The rat bones were cut transversely with a sharp scalpel at two points 5mm proximal and 5mm distal to the center of the fracture callus. Another cut was then made at the center where the original fracture had been determined from the X-ray assessments thereby creating two half callus specimens. Mouse calluses were isolated in the same manner but were left intact. After dehydration in graded concentrations of ethanol to 100%, the specimens were transferred to xylene, and embedded in a step-wise manner under vacuum in 50% xylene paraffin, then 100% paraffin. The two halves of the rat callus were positioned in a single block of low-melt paraffin with the fracture centers facing the cutting surface. The mouse calluses were embedded intact with the distal end (end closest to the tibial joint) facing the cutting surface. A counting microtome was used such that the total linear distance that had been sectioned through a block could be monitored. Five micron thick paraffin sections were cut and placed on poly L-lysine coated slides, dried overnight and used immediately or stored at 4°C.

Histomorphometric Parameters and Sampling Scheme

Three rat or five mouse bones were used for each time point of the histomorphometric analysis. Twelve to fifteen, 5 μm-thick serial sections were taken at 100μm increments across the entire length of each callus (~6000μm). In this manner a series of ~60 segments containing groups of serial sections were obtained that spanned the complete length of the callus. The positions of each segment from which serial sections was taken is denoted relative to the center (C) which is the site of the fracture and various segments containing groups of serial sections are enumerated in distances proximal (P) or distal (D) to the center as defined by the original anatomy of the femur. The histomorphometric sampling schemes that were used to examine callus morphogenesis and the progression of healing are summarized in Figure 1 A and B. The histomorphometric indices that were examined were as previously described[13] and included: callus diameter (CDm), callus areas (C/Ar) cartilage areas (Cg/Ar), void areas (V/Ar) [inclusive of empty space and hematopoietic elements], total osseous tissue TOT/Ar [inclusive of the original cortical bone that was present prior to the fracture new cortical

bone, trabecular bone and lining cells], and osteoclast density (Oc/Ar). The abbreviations, nomenclature and unit measurements are in accordance with the currently used standards for histomorphometry of intact bone.[14,15]

Staining Methods and Image Collection

Sections were stained with Safranin O-Fast Green as previously described[16] to discriminate mature cartilage from bone and non-cartilage connective tissues.[17] Tartrate resistant acid phosphatase (TRAP), a marker for osteoclasts, was detected using an azo-dye coupling method with the slight modification of fast red violet LB salt (Sigma F-3381, Sigma Chemicals, St. Louis, MO) replacing the fast red TR salt. Each section was photographed with an Olympus BX51 light microscope attached to a digital camera at 10.25X and downloaded into an Image-Pro Plus Version 4.1.0.0 for Windows program. An area of interest (AOI) was created by loading a uniform box (5mm x 7.9mm) onto the photograph and centering the callus within the box. The bone was then outlined within the uniform AOI, excluding any muscle, soft tissue or periosteum. Using a color match program, the total area of cartilage (red) and bone (green) was initially identified quantified using a filter range of 573.9μm-5.74e+03μm. Subsequently colored matched areas defining specific tissues were individually assessed and final areas were hand traced. Mean values were calculated for specimens sampled from each bone and then used to create group means, standard deviations and standard errors both with respect to time after fracture and animal group.

For measuring either TRAP-stained cells, contiguous areas were sampled collecting as many as 7 micrographs for each transverse section, such that when overlapped with each other they spanned the width of the callus (Figure 1C). Microscopic images were captured as described above and adjacent micrographs (10.5mm x 7.8mm) were taken using the 20X objective and downloaded onto an Image-Pro Plus Version 4.1.0.0 for Windows program. Using a color match program, the osteoclasts from each photograph were quantified using a spot filter and a pre-defined pixel value that defined the lower and upper dimensions for the spots counted. Mean values of TRAP positive cells per callus age groups were calculated from cross sectional measurements taken at 1000 micron increments across the total longitudinal distance of each callus (N=37-49

micrographs per callus). The numbers from the multiple images per group were combined and specimen means calculated and used to create group means, standard deviations and standard errors.

Statistical Methods

Each callus was divided into approximately 30 segments proximal and 30 segments distal with each segment of serial sections taken at 100 μm intervals from the anatomic center as defined by the fracture. This is shown schematically in Figure 1A. Each segment contained a group of 12-15 serial 5μm sections. One section from each segment was then analyzed such that the entire length of each callus (total of ~60 sections one from each segment across the entire length of the callus) were used for quantitative measurements. The statistical variability in the various histological measurements in each callus was obtained by determining the mean values from the measurements made from the ~ 60 sections taken across the entire length of each of the calluses. This was then used to define the so-called reference value for each of the measurements. The 95% percent confidence interval was calculated around each reference value and was used to define the minimal number of sections per callus to accurately predict values for each measurement. The minimal number of segments from which sections should be taken was estimated by taking the sections from increasing increments (every 2nd, 3rd 4th etc segments) starting with the central proximal (P1) and distal (D1) sections. This is presented diagrammatically in figure 1 A, with variations in the sampling measurements denoted at progressively larger increments within the segments denoted by Xs. The mean values for each of the primary anatomical measurements were then computed for each set of sample and compared to the 95% confidence interval for the respective reference value. From these preliminary statistical analyses it was determined that sampling at an increment of not greater than 500 μm and spaced uniformly across the complete longitudinal distance of the callus accurately fell within the 95% confidence interval of the references for each of our measurements. The means and standard deviations between all histological measurements in the data presented in this study therefore were all derived from a sampling increment of 500 μm uniformly spaced across the length of the callus.

It should be noted as well that other sampling schemes such as taking sections just from segments around the center for example do not provide means that fit with the confidence interval with as few a number of sections as uniformly spacing the increment across the entire length of the callus. Power analysis for carrying out future studies were also determined (data not shown).

In Situ Hybridization

Five micron-thick sections were placed on poly L-lysine or 15% Bond-fast glue (Manco Inc., Avon, OH) coated slides, dried overnight and used immediately or stored at 4°C. Both antisense and sense control, ^{35}S-labeled, cRNA probes were used for hybridization. Linear cDNA sequences were incubated with either T7 or SP6 RNA polymerase in the presence of ^{35}S-UTP (New England Nuclear, Boston, MA), unlabeled nucleotides, 10mM DTT, and Rnasin RNase inhibitor (Promega, Madison, WI). Labeled cRNA probes were purified using Mini Quick Spin RNA columns (Roche Diagnostics, Indianapolis, CA). Prehybridization: Slides were deparaffinized in xylenes followed by rehydration in graded ethanol solutions, rinsed in 0.85% NaC1 (5 minutes) and 1X PBS (5 min), and treated with proteinase K (20µg/ml) for 8 minutes at 37ºC. Slides were dipped successively in 1X PBS (5 min), 4% paraformaldehyde (5 minutes), acetylated in 0.25% acetic anhydride in 100 mM triethanolamine (10 minutes), washed in 1X PBS (5 minutes), 0.85% NaC1 (5 minutes), dehydrated in graded ethanol solutions, and air dried. Hybridization: Hybridization solution contains 50% deionized formamide, 0.3M NaCL, 20mM Tris-HC1 (pH 7.5), 5mM Na_2EDTA (pH 8.0), 10% dextran sulfate, 1X Denhardt's solution, 0.5 mg/ml total yeast RNA, and 100mM DTT. ^{35}S-labeled cRNA probes are heated at 80ºC for two minutes and placed on ice. Hybridization solution containing ^{35}S-labeled probe at $5x10^4$cpm/µl was added to each slide in a 50 - 60µl volume, a plastic HybriSlip (Research Products International, Mt. Prospect, IL, USA) was placed on each slide, and the slides were incubated at 52ºC for 16 hours. After hybridization, slides were washed in 5X SSC for 30 min at 50ºC, 2X SSC with 50% deionized formamide for 20 min at 65ºC, and rinsed twice in 10X STE, 10min each, at 37ºC. Slides were then treated with a 20µg/ml solution of RNase A (Pharmacia Biotech, Piscataway, NJ) for 30 minutes at 37ºC, washed in 2X and 0.1X SSC for five minutes each, dehydrated in graded ethanol, and air dried. Autoradiography: Air dried slides were dipped in Kodak NTB-2

emulsion (Eastman Kodak, Rochester, NY), drained, air-dried for 1 hour, and placed in a light-proof container with desiccant at 4ºC for 2-3 weeks. Slides were developed in Kodak D-19 developer, fixed in Kodak fixer, and counterstained with Fast Green and Safranin-O.

Three Dimensional Reconstructions

Three dimensional reconstructions were performed using the Amira 3.0 software system for 3D visualization data analysis and 3D geometric reconstruction (Visual Concepts GmbH, Company, Konrad-Zuse-Zentrum (ZIB), Research Institute Berlin, Germany). All image modifications were performed in Adobe Photoshop Software, (Adobe Systems, Incorporated; San Jose, CA USA). In order to use the color recognition operations employed during the 3D reconstruction process, soft tissue areas surrounding the exteriors of the calluses were digitally removed from individual images by hand tracing tissue perimeters in the Photoshop program, and cutting these areas from the images. Amira 3.0 3D reconstruction software is unable to recognize multi-channel images that are acquired initially, but subsequent grayscale outputs yield enough contrast to differentiate the tissues of interest. In order to maximize the color contrast differentials within a gray scale image, the color differentials were first digitally extracted to optimize staining contrasts. Since areas of mature cartilage tissue stained bright red with Safranin O/ Fast Green areas were hand traced and the green channel was first extracted from the primary RGB image thereby enabling the cartilage to be easily contrasted as black areas in separate grayscale images. This high degree of contrast in the green channel makes this staining property ideal for accurate measurements using image thresholding techniques. For cortical bone measurements and image discriminations these areas were outlined in each slice using a manual segmentation tool. Once individual images were modified they were imported into Amira software program and the slices manually aligned using edge to edge matching of the edges from the surgical pin hole in the marrow cavity using Amira's slice alignment editor. The slice aligner permits user visualization of two consecutive slices at a time, each exhibiting opposite contrast. This yields a 50% grey image representing two perfectly matched, overlapping images. The editor allows for both slices to be aligned with either the previous or the next slice as well as the ability to manipulate the entire stack of slices in order to center the field of view within a bounding box.

In order to visualize 3D surfaces, the different tissues were labeled or 'segmented' using the segmentation editor in the software program. Individual sets of labels were created for cartilage, cortical bone, the callus as a whole and for the space between the trabeculae. The segmentation editor allows for both manual and automated segmentation. For most tissues it was possible to use the automated segmentation to label slices using thresholding. Thresholding provides a simple and fast method of labeling without false positive results. False positives were easily identified by comparing the labeled images with the originals. The non-resampled stack of slices is used for this, and the labels are later resampled to maximize accuracy.

The 3 D spatial distribution of collagen type I - and collagen type II - expressing cells in the healing fracture calluses were visualized using in situ hybridization. To simplify the reconstructions of the collagen I and collagen II in situ hybridizations, a color select was performed for these markers in Adobe Photoshop 5.5 using dark field images. As with the color staining, this pre-optimization of the images was used to enhance the color differentials in the grayscale images. Through thresholding a binary image is produced, thereby simplifying the segmentation process. The separate stacks of slices for collagen I and collagen II in situ hybridization images were inserted into the existent stacks generated from the three rendering of the light images, paying careful attention to the spatial coordinates to ensure a proper overlap.

Volumes were obtained from each reconstructed surface using an automated volume measurement function in Amira. The scale was determined by comparing the known width of each image with the measurement determined by Amira for the width of the bounding box. A stage micrometer was used to determine the actual width of each image in Image-Pro Plus. The scale was thus determined as being 100μm = 1.32 Amira Units, and hence 1 Amira Unit^3 = 0.000435 mm^3.

RESULTS

Quantitative Analysis of the Spatial Morphogenesis of Callus Development

The cross sectional diameters and area measurements of the calluses reflect the remodeling of the tissues as they diminish from their peak dimensions towards their original anatomical sizes and configurations (Figure 2). For the rat, maximal fracture callus tissue areas were observed at 21 days after which their size

progressively diminshed over the time-course of healing. It is interesting to note that while the medial-lateral diameters showed the greatest changes over the healing period, the posterior-anterior diameters showed a smaller variation with maximal diameters observed between 14 and 21 days after fracture. These gross measurements can be used to develop a general understanding of the overall rate and spatial distribution of tissue formation (peak size of calluses) and callus remodeling (change in size and progression back to control values) and provide a means for relating quantifiable histological parameters to biomechanical properties including strength, stiffness, and moments of inertia.

The overall progression of skeletal morphogenesis was next assessed by measurement of the resorption of cartilage during the endochondral phase of healing. Total osseous tissue (existing cortical bone, new trabecular bone, new osteoid tissue, and the void space that includes the bone marrow cavity, hematopoietic elements and empty, unstained space) is a reasonable measure of overall primary and secondary bone formation (Figure 3). Measurement of void area in relationship to the amounts of total osseous tissues and cartilage was particularly informative as this measurement provided another gross assessment of the rates of initial cartilage resorption. This is because the void space, which is composed of hematopoietic elements and marrow space, does not appear within the callus until mineralized cartilage begins to be remodeled.

The most striking aspect of these data was that the formation of the cartilage tissues takes place in an asymmetric manner with more cartilage formed on the distal than the proximal side of the callus. This asymmetry was also reflected in the overall proximal to distal area and diameter measuements of the callus as seen in Figure 2. Comparison of the measurements among three primary histological parameters Cg, TOT and Vd at 14, 21, and 35 days demonstrated that spatial asymmetry in the intial endochondral distribution affected both the pattern of tissue remodeling, and the pattern of osseous tissue formation over the time course of healing. In this context, the measurement of void area provided a retrospective spatial picture of where remodeling had already occurred. Intially the void areas were observed at the sites most proximal and distal to the fracture. However, as healing proceded, the areas of remodeling progressed inward and the void areas were seen flanking the regions adjacent to the fracture at the center of the callus, where the areas of cartilage persisted (Figure 3A compares void measurements at days 14 and 35).

Using the means from the entrire set of measurements, the percent composition of cartilage to total osseous tissue to void area were determined (Figure 3 panel B). While it has generally been assumed that cartilage makes up a very high percentage of the tissue content of fracture callus, the cartilagenous component comprised only ~10 to 15% of the total tissue content at 14 days post fracture. However, in some of the distal sections close to the center cartilage consituted approximately 30% of the callus area. As the healing progressed and cartilage was resorbed and there were increases in the percent of total osseous tissue and void area. This observation regarding the total amount of cartilage (10 to 15%) is also consistent with that seen at the peak period of callus formation in mouse femur calluses produced in the same experimental manner (data not shown).

The spatial pattern of tissue remodeling was further examined by assessing osteoclast density (OC/Ar) throughout the callus using TRAP staining (Figure 3C). Detailed data from 21 and 35 day calluses are presented. A comparison of the spatial distribution of osteoclasts with the spatial distribution of cartilage and void areas at 21 days provides a consistent picture of the retrospective spatial pattern of cartilage tissue resorption. The areas containing the highest density of osteoclasts were situated toward both the proximal and distal edges of the callus with a high density in the areas of cartilage which will undergo resorption. As these areas are remodeled, they will be replaced with void areas and trabecular bone. From a quantitative perspective there is almost a 5:1 ratio in the total density of osteoclasts during the active periods of cartilage remodeling at day 21 than during primary and secondary bone remodeling that predominates at day 35. By 35 days, the distribution of osteoclasts throughout the callus is relatively uniform except at the most proximal edges.

Three Dimensional Reconstruction of Callus Morphogenesis

Three dimensional reconstructions of rat fracture calluses were generated from serial histological sections taken at ~100 □m increments (all 60 sections), spanning ~ 6 mm, of a 14 day callus (Figure 4). Four representative slices, two from the proximal and two from the distal halves of the fracture callus, are presented in the bottom panel B. The three dimensional renderings of these data validate the two dimensional compositional assessments (see below Table 1) and more clearly show that the cartilage components of the callus were formed in an asymmetric manner, with the majority of the cartilage formed distal to the fracture. A

second reconstruction of a different fourteen day callus is seen in panel C. However, this rendering was stretched so that a 1:5 to 1:0 aspect ratio is presented to depict the asymmetry of the tissue in a more exaggerated manner. Two separate anatomical perspectives, viewing the tissue from either the medial or lateral surfaces, again show the asymmetry in cartilage development in the proximal and distal orientations but extend this the asymmetry into the medial/lateral, posterior/anterior dimensions as well. The cartilaginous component of the callus wraps around the cortical bone toward the medial side as it develops toward the proximal end of the callus. Whereas the signals that initiate repair either arise from the marrow or are released from the injured bone matrix around the fracture, the spatial morphogenesis of the callus is regulated by other extrinsic or intrinsic factors that lead to asymmetry of tissue development. The asymmetric configuration of the callus continues to be observed throughout the rest of the period of the bone healing as seen in the three dimensional renderings of the callus at 21 days, with very little cartilage now remaining on the proximal side of the fracture (Figure 4D).

An assessment of how the fracture calluses were spatially remodeled over time was carried out by three dimensional reconstructions 35 days post fracture (Figure 5). One of the most striking features of these reconstructions was observed in the spatial geometry of the newly formed bone within the 35 day callus. By 35 days no observable cartilage remained in the callus (Figure 5A-B). These studies show that the original central space of the callus, which was occupied by cartilage, has now been replaced with trabeculated bone tissue that is surrounded by an outer and inner shell of new bone (Figure 5C). The outer shell formed as new bone grew over the cartilage and became the new periosteal margin adjacent to the muscle. The inner shell formed as a new surface adjacent to the original cortex and is representative of the periosteal response (Figure 5C). The original cortices that underlied the new bone surface were now undergoing extensive resorption and become the site of new blood vessel in growth. Eventually, both the original cortices and the new layer of bone became remodeled and were replaced with a continuous volume of trabeculated bone underlying the new cortical shell. The asymmetry of the bone formation continues to be obvious during this phase of callus morphogenesis as seen in the cross sectional views. There is a very small amount of trabeculated bone bridging the inner and outer shell of the cortices in the proximal view but an extensive network of trabeculated bone when viewed from the distal orientation.

The three dimensional renderings were used to calculate the percent composition of the three major tissue types within the callus. These were based on comparing the determined volumes with the average area fractions calculated from the two dimensional analyses carried across the serial sections. The results for these analyses are summarized in Table 1 for determinations made from the 21 day specimens. As can be seen, the 2 dimensional analysis accurately (within 1-2%) reflects the determined percentages of 3 dimensional volumes validating both the internal consistency and accuracy of both sets of determinations made from the histological measurements.

Three Dimensional Reconstruction of the Spatial Pattern of Collagen mRNA Expression

Using in situ hybridization the spatial pattern of collagen types I and II gene expression were three dimensionally reconstructed as a means of identifying the spatial patterns of biological activity of specific populations of cells in the callus tissue. For these studies murine femur fractures were generated. Both light and dark field images show the fidelity of the in situ hybridizations for the col1a1 and col2a1 mRNAs (Figure 6). The intense and very specific localization of the two probes with respect to either bone lining cells on the nascent trabecular surfaces or at the interface with chondrocytes adjacent to these surfaces are shown.

In Figure 7, murine femur fracture callus was reconstructed using sections taken at ~500□m increments spanning ~6 mm of the callus. Representative proximal and distal serial sections are presented (using light microscopy/safranin O staining for orientation) for each hybridization probe shown in Panel A. The lower panels depict both the reconstruction of the cortical bone in relation to cartilage (Panel B) and the expression of col1A1 and col2a1 in these tissues (Panes l D and E). An end on image is shown to provide confirmation of the alignment of serial reconstructions based on the position of the medullary pin (Panel C). Mouse femoral fracture callus showed the distal-lateral asymmetric distribution of cartilage similar to that observed for the rat femur. As expected, areas of col2a1 expression were spatially aligned with the cartilage. The expression of col2a1 was confined to the central areas around the fracture line but not the areas of callus more peripheral to the fracture. In contrast, col1a1 expression was uniformly seen on either side of the fracture and was distinctly excluded from the regions around the fracture site. The col1a1 expression was spatially adjacent to all of the

areas in which cartilage was observed and col1a1 was expressed in a mirror-like fashion on opposite surfaces from cartilage.

DISCUSSION

The morphogenesis of skeletal tissues during development is controlled by spatio-temporal relationships between various cells types and their secreted morphogens, as well as mechanical cues in the microenvironment. During long bone development involving an endochondral process these spatial arrangements are defined by both the patterns of linear growth of the tissues as well as the weight-bearing demands these tissues will be required to meet. While it is generally accepted that the endochondral bone formation during fracture healing recapitulates many of the molecular events that control embryological and post-natal growth[1,23], the well-defined spatial arrangements that define tissue morphogenesis during bone growth are not as easily discernable within a fracture callus. The question that arises is how the events of spatial morphogenesis intrinsic to long-bone development differ from those that are involved during healing and regeneration.

Most histological assessments of fracture callus formation have used longitudinal sections (sagittal, coronal) which have lead to a simplistic view of callus morphogenesis as a uniform ring of cartilage that initially forms around the fracture[18]. However, many long bones are ellipsoid or have flattened surfaces and these configurations affect the spatial parameters of morphogenesis. Indeed, in the course of our attempts to perform histomorphometric analyses of fracture healing, we observed that measurements of cartilage and bone composition, as well as measurements of callus sectional area varied tremendously among longitudinal sections.[17] In order to circumvent these problems, a serial, transverse sampling method was used in the experiments reported in this study.

The most striking finding of the quantitative analysis of tissue composition was the degree of spatial variability of cartilage formed during fracture healing. The cartilage tissue spiraled around the femoral shaft in a proximal to distal manner. This spatial pattern suggests that there is a much greater complexity among the biological and biomechanical factors that initiate and regulate the endochondral processes of fracture healing compared to those that occur in the later phases of bone remodeling. This inherent complexity is reflected in the

much greater number of uniquely expressed mRNAs in fracture callus compared with unfractured bone as determined by large scale transcriptional profiling.[20] This variability may also be the cause of the statistical variation in the biomechanical properties of endochondral fracture callus at early time points.[21,22,23] The most likely explanation for this variation is related to the anisotropy produced by spatial irregularities in the formation of callus tissues. Finally, it may be speculated that the complexity of the endochondral process makes the transition through this phase of bone healing an extremely sensitive index of the progression of normal healing. Indeed, delays or failures to progress through the chondrogenic stages of fracture healing have been associated with the development of delayed and nonunions in both clinical studies[18] and investigations in animals.[17,24,25]

Two of the most interesting findings from the present studies are the reproducible asymmetric pattern in which cartilage develops during callus formation and the spatial mechanisms by which the callus is remodeled back to its pre-fracture size. In the case of the spatial pattern of cartilage tissue development, our analyses demonstrated that the majority of the cartilage formed distally and laterally to the fracture with periosteal bone formation being the greatest on proximal lateral surfaces. This asymmetry was conserved across species in both mice and rats. The initial asymmetry in tissue formation subsequently affected the spatial patterns of cartilage resorption that were observed as the chondrocytes underwent hypertrophic maturation. Thus, regions of chondrocyte maturation and subsequent resorption progressed from the edges inward with regions flanking the proximal fracture undergoing resorption first followed by those areas distal to the fracture. As to the role of intrinsic versus extrinsic factors controlling the unique pattern of tissue formation in the callus, it is important to note that femurs of several mammalian species appear to grow predominantly from the distal physis.[26,27,28] While we do not report on data from the tibia we have observed in other experiments that tibial fracture callus shows more cartilage within the proximal halves of the callus and this bone grows preferentially from the proximal end.[27] These data suggest that the proximal to distal distribution of cartilage may be an intrinsic feature of the way skeletal tissues form during fracture healing and may be bone-specific that are related to additional factors that are developmentally controlled such as blood supply, soft tissue or muscular coverage[9,30] and mechanical demand. Indeed, one of the most important extrinsic factors is the biomechanical

environment, which has been shown both through theoretical considerations [31,32] and empirical experimentation to be crucial to cartilage development. [33-37]

The final aspect of these data to discuss is the spatial pattern by which woven bone is remodeled to its original cortical dimensions. Once the cartilage component of the callus has been resorbed there are two new surfaces of bone: an inner surface that has grown over the original cortex and an outer thinner layer that has encapsulated the callus and forms the new interface with the periosteum. A trabecular structure bridges these surfaces in the space that was occupied by cartilage. The outer shell, because it is located far from the geometric center of the bone, will be responsible for the majority of weight bearing.[38] This outer shell is connected to the original cortex via trabecular-like struts which appear to provide sufficient support in order that it can function to stabilize the fracture. This represents an efficient mechanism, using minimal material, to rapidly restore biomechanical stiffness and strength, while allowing for remodeling on internal surfaces. A similar pattern of morphological expansion has been observed during the early phase of rapidly growing animals such as inbred mice [39]. Unlike long-bone expansion in which there is a balance between periosteal appositional growth and bone resorption at the endosteal surface, the remodeling of fracture callus uses different and unique spatial mechanism to model and remodel from the outer surface inward balancing external removal with the addition of bone on internal surfaces. This aspect of fracture healing is perhaps the most structurally complicated and the ability to construct a simple model to explain how this takes place is very challenging. As noted from these results, more bone forms distal to the fracture site during femoral healing and proximal to the fracture site in the tibia. Further investigations will be required in order to better understand the complex interplay of each of these processes.

REFERENCES

[1] Gerstenfeld LC, Cullinane DM, Barnes GL, Graves DT, Einhorn TA 2003 Fracture healing as a post-natal developmental process: molecular, spatial, and temporal aspects of its regulation. J Cell Biochem 88:873-884.

[2] Einhorn T, Lee C 2001 Bone regeneration: new findings and potential clinical applications. J Am Acad Orthop Surg 9:157-165.

[3] Ferguson C, Alpern E, Miclau T, Helms JA 1999 Does adult fracture repair recapitulate embryonic skeletal formation? Mech Dev 87:57-66.

[4] Einhorn TA, Majeska RJ, Rush EB, Levine PM, Horowitz MC 1995 The expression of cytokine activity by fracture callus. J Bone Miner Res 10:1272-1281.

[5] Kon T, Cho TJ, Aizawa T, Yamazaki M, Nooh N, Graves D, Gerstenfeld LC, Einhorn TA 2001 Expression of osteoprotegerin, receptor activator of NF-kappa B ligand (osteoprotegerin ligand) and related proinflammatory cytokines during fracture healing. J Bone Miner Res 16:1004-1014.

[6] Street J, Bao M, deGuzman L, Bunting S, Peale FV Jr, Ferrara N, Steinmetz H, Hoeffel J, Cleland JL, Daugherty A, van Bruggen N, Redmond HP, Carano RA, Filvaroff EH 2002 Vascular endothelial growth factor stimulates bone repair by promoting angiogenesis and bone turnover. Proc Natl Acad Sci USA 99:9656-9661.

[7] Lehmann W, Edgar CM, Wang K, Cho TJ, Barnes GL, Kakar S, Graves DT, Rueger JM, Gerstenfeld LC, Einhorn TA 2005 Tumor necrosis factor alpha (TNF-alpha) coordinately regulates the expression of specific matrix metalloproteinases (MMPS) and angiogenic factors during fracture healing. Bone 36:300-310.

[8] Gerber HP, Ferrara N 2000 Angiogenesis and bone growth. Trends Cardiovasc Med 10:223-228.

[9] Richman C, Kutilek S, Miyakoshi N, Srivastava AK, Beamer WG, Donahue LR, Rosen CJ, Wergedal JE, Baylink DJ, Mohan S 2001 Postnatal and pubertal skeletal changes contribute predominantly to the differences in peak bone density between C3H/HeJ and C57BL/6J mice. J Bone Miner Res 16:386-397.

[10] Jepsen KJ, Akkus O, Majeska RJ, Nadeau JH 2003 Hierarchical relationship between genetically determined bone traits and whole bone mechanical properties in inbred mice. Mammal Genome 14(2):97-104.

[11] Lang DH, Sharkey NA, Mack HA, Vogler GP, Vandenbergh DJ, Blizard DA, Stout JT, McClearn GE 2005 Quantitative trait loci analysis of structural and material skeletal phenotypes in C57BL/6J and DBA/2 second-generation and recombinant inbred mice. J Bone Miner Res 20:88-99.

[12] Bonnarens F, Einhorn TA 1984 Production of a standard closed fracture in laboratory animal bone. J Orthop Res 2:97-101

[13] Gerstenfeld LC, Wronski TJ, Hollinger JO, Einhorn TA 2005 Perspective: The application of histomorphometric methods to the study of bone repair. J Bone Miner Res 20:1715-1722.

[14] Parfitt AM, Drezner MK, Glorieux FH, Kanis JA, Malluche H, Meunier PJ, Ott SM, Recker RR 1987 Bone histomorphometry: standardization of nomenclature, symbols and units. J Bone Mineral Res 2:595-610.

[15] Eriksen EF 1986 Normal and pathological remodeling of human trabecular bone: three dimensional reconstruction of remodeling sequence in normals and metabolic bone disease. Endocrin Rev 7:379-408.

[16] Armed Forces Institute of Pathology Laboratory 1992 Methods in Histotechnology. American Registry of Pathology, Washington, DC, USA.

[17] Gerstenfeld LC, Cho T-J, Kon T, Aizawa T, Tsay A, Barnes GL, Graves DT, and Einhorn TA 2003 Impaired fracture healing in the absence of TNF-□ signaling: the role of TNF-□ in endochondral cartilage resorption. J Bone Min Res 18:1584-1592.

[18] Edwards RB, Lopez MJ, Markel MD 2003 Histological analysis of bone healing. In: An YH, Martin KL (eds.) Handbook of Histology Methods for Bone and Cartilage. Humana Press, Totowa, NJ, USA. pp. 375-389.

[20] Wang K, Vishwanath P, Eichler G, Al-Sebaei MO, Edgar CM, Einhorn TA, Smith TF, and Gerstenfeld LC 2005 Large scale transcriptional profile analysis across fracture healing identifies the temporal relationships between metalloproteinase and ADAMTS mRNA expression. Matrix Biology (In Press).

[21] Gerstenfeld LC, Thiede M, Seibert K, Mielke C, Phippard D, Svagr B, Cullinane D, Einhorn TA 2003 Differential inhibition of fracture healing by non-selective and cyclooxygenase-2 selective non-steroidal anti-inflammatory drugs. J Orthop Res 21:670-675.

[22] Einhorn TA, Majeska RJ, Mohaideen A, Kagel EM, Bouxsein ML, Turek TJ, Wozney JM 2003 A single percutaneous injection of recombinant human bone morphogenetic protein-2 accelerates fracture repair. J Bone Joint Surg Am 85-A:1425-1435.

[23] Alkhiary YM, Gerstenfeld LC, Krall E, Westmore M, Sato M, Mitlak BH, Einhorn TA, 2005 Enhancement of experimental fracture healing by systemic administration of recombinant human parathyroid hormone (PTH 1-34). J Bone Joint Surg Am 87:731-741.

[24] Simon AM, Manigrasso MB, O'Connor JP 2002 Cyclo-oxygenase 2 function is essential for bone fracture healing. J Bone Miner Res 17:963-976.

[25] Zhang X, Schwarz EM, Young DA, Puzas JE, Rosier RN, O'Keefe RJ 2002 Cyclooxygenase-2 regulates mesenchymal cell differentiation into the osteoblast lineage and is critically involved in bone repair. J Clin Invest 109:1405-1415.

[26] Farnum CE, Lee AO, O'Hara K, Wilsman NJ 2003 Effect of short-term fasting on bone elongation rates: an analysis of catch-up growth in young male rats. Pediatr Res 53:33-41.

[27] Kuhn JL, DeLacey JH, Leenellett EE 1996 Relationship between bone growth rate and hypertrophic chondrocyte volume in New Zealand white rabbits of varying ages. J Orthop Res 14:706-711.

[28] Pritchett JW 1992 Longitudinal growth and growth-plate activity in the lower extremity. Clin Orthop Relat Res 275:274-279.

[29] Einhorn TA 1998 The cell and molecular biology of fracture healing. Clin Orthop 355S:S7-S21.

[30] Utvag SE, Grundnes O, Rindal DB, Reikeras O 2003 Influence of extensive muscle injury on fracture healing in rat tibia. J Orthop Trauma 17:430-435.

[31] Carter DR, Blenman PR, Beaupre GS 1988 Correlations between mechanical stress history and tissue differentiation in initial fracture healing. J Orthop Res 6:736-748.

[32] Carter DR, Wong M, Orr TE 1991 Musculoskeletal ontogeny, phylogeny, and functional adaptation. J Biomech 24:3-16.

[33] Le AX, Miclau T, Hu D, Helms JA 2001 Molecular aspects of healing in stabilized and non-stabilized fractures. J Orthop Res 19:78-84.

[34] Cullinane DM, Fredrick A, Eisenberg SR, Pacicca D, Elman MV, Lee C, Salisbury K, Gerstenfeld LC, Einhorn TA 2002 Induction of Articular-like Cartilage and a Joint-like Structure by Controlled Motion in an Experimental Mid-Femoral Defect. J Orthop Res 20:579-586.

[35] Cullinane DM, Salisbury KT, Alkhiary Y, Eisenberg S, Gerstenfeld L, Einhorn TA 2003 Effects of the local mechanical environment on vertebrate tissue differentiation during repair: does repair recapitulate development? J Exp Biol 206:2459-2471.

[36] Claes L, Eckert-Hubner K, Augat P 2002 The effect of mechanical stability on local vascularization and tissue differentiation in callus healing. J Orthop Res 20:1099-1105.

[37] Smith-Adaline EA, Volkman SK, Ignelzi MA Jr, Slade J, Platte S, Goldstein SA 2004 Mechanical environment alters tissue formation patterns during fracture repair. J Orthop Res 22:1079-1085.

[38] van der Meulen MC, Jepsen KJ, Mikic B 2001 Understanding bone strength: size isn't everything. Bone 29:101-104.

[39] Price C, Herman BC, Lufkin T, Goldman HM, Jepsen KJ 2005 Genetic variation in bone growth patterns defines adult mouse bone fragility. J Bone Miner Res 20:1983-1991.

FIGURE LEGENDS

Figure 1. Schematic presentation of methodological standardization for histomorphometric assessment of fracture callus. In these black and white pictures areas stained red with the Safranin O-Fast Green appear dark grey to black. Panel A) Diagram of the sampling approaches used to quantify histological measurements across a fracture callus. The fracture callus was divided into segments, which were denoted as proximal or distal to the center of the callus. Each segment was 100 μm apart. Sections were sampled within segments that were progressively spaced at larger increments, every segment, every other segment, etc. as denoted by the Xs across the whole proximal to distal orientation of the callus (Materials in Methods, Statistical Methods). Panel B) Representative set of four transverse serial histological sections taken at ~2000 μm increments in the proximal (P) to distal (D) orientation from the fracture line of a 14 day post fracture callus of a rat femur. Photomicrographs were taken at 25 x magnification. Panel C) Sampling method that was used to obtain micrographs for analysis for measurements of osteoclasts. A representative transverse section is presented. Micrographs were taken consecutively at 6-7 arbitrary positions as boxed across the diameter of the callus. Transverse increments are then taken across the entire length of the callus within segments at 1000 μm increments.

Figure 2. Comparison of mean callus area measurements at 14, 21 and 35 days post fracture in rat femur fracture calluses. Panel A) Graphical analysis of the mean total callus areas from 1000μm increments from the proximal to distal sides of the callus as a function of time after fracture. Panel B) Comparison of the mean cross sectional measurements of callus diameters in the medial/lateral or posterior/anterior dimensions as a function of time after fracture. Panel C) Comparison of the mean callus areas as a function of time after fracture. Values are based on the mean taken from the minimal increment within the 95% confidence interval of the reference. † $p < .05$ between 35 days and 14 days. * $p < .05$ between 35 days and 21 days.

Figure 3. Comparisons of the histomorphometric measurements of rat femur callus tissue compositions at 14, 21, and 35 days post fracture. Panel A) Graphical analysis of the primary histological measurements assessed at

500□m increments from the proximal to distal sides of the callus. Panel B) Graphical analysis of Cg, TOT and Vd as a function of time. Comparison of the mean callus areas as function of time after fracture. Values are based on the mean taken from the minimal increment within the 95% confidence interval of the reference. Error bar = SD of the means from three calluses at each time point † $p < .05$ between 35 days and 14 days. * $p < .05$ between 35 days and 21 days. Panel C) Quantification of osteoclasts within fracture callus at 21 days post fracture. Left panel shows the mean total numbers of osteoclasts per area at 1000 μm increments across the proximal to distal length of the calluses from the center. Values from either 21 or 35 days post fracture are shown. Right panel presents overall mean osteoclast number per unit area when averaged over the entire length of the callus. Increments are averaged values from the mean additive values from the proximal and distal increments at the center 1000, 2000, and 3000 μm. Error bar = SD.

Figure 4. Reconstruction of a rat femoral fracture callus, 14 days post fracture. Three dimensional reconstructions were made from serial sections taken every 100 microns. Panel A) Representative 3D reconstruction of the cartilage tissues within the callus relative to the original cortical bone. The cortical bone is denoted by grey to white stained areas relative to mature cartilage denoted dark grey to black. The positions of the levels of individual slices depicted in panel A are correlated with those in Panel B) The anatomical orientations of four slices through the callus tissue. The positions of the slices as denoted in panel A are each shown in panel B. Panels C) Demonstration of the geometric asymmetry of the callus formation. Medial and lateral presentations of a second reconstruction of a 14 day rat callus are shown in a 1:1.5 aspect ratio. Arrows denote orientation of rotation and volume distribution of cartilage. Panel D) Reconstruction of the cortical bone (light grey to white) relative to mature cartilage (dark grey to black) within the soft callus of a 21 day callus shown for femur fracture of the rat.

Figure 5. Reconstructions of rat fracture calluses at 35 days. Panel A) represents cortical bone as described in figure 6. No cartilage was observed in this specimen. Panel B) Slices from selected proximal and distal positions are as denoted in figure 6. Panel C) Reconstructions of rat femur calluses at 35 days. The left panel

depicts an end on view from the distal orientation of the entire callus volume. The original cortical bone is denoted with (*). Middle and right panels present proximal and distal views of the external shell of new bone and the trabecular structure that has formed during the resorption of the regions of original endochondral bone. Boxed areas are regions in which secondary remodeling has completely replaced the original cortical bone with a continuum of trabecular bone.

Figure 6. Three dimensional reconstruction of mouse femur fractures and collagen types I and II gene expression. Panel A) Representative light and dark field images of micrographs taken of in situ hybridizations. Top micrograph depicts 40x magnification light field of a Saffrin O / Fast Green stained section from a 7 day murine femur fracture callus. Middle and bottom panels are dark fields from serial sections hybridized respectively with col1a1 and col2a1 DNA probes. Boxed area corresponds to that depicted in the 100x magnifications seen in panels on the Right. Alternating images from top to bottom show light field and dark fields from consecutive serial slides hybridized respectively with a probe for col1a1 and col2a1. Identical areas of silver grain development seen in the light field and matched dark fields are indicated with arrows.

Figure 7. Spatial reconstruction of tissue structure and collagen gene expression of 7 day murine femur fracture calluses. Panel A) Micrographic images (40x magnification) of light (saffrin O/ fast green) and dark field (in situ hybridization) images of serial sections of calluses made at 500μM increments over a 6 mm distance. Representative serial histological were hybridized with probes for col1a1 and col2a1. The serial sections were then reconstructed Panel B) Reconstruction of the spatial relationship of the cartilage tissue within the callus in relation to the cortical bone. Panel C) Flat surface reconstruction showing end-on view of the total volume. Panel D) col1a1 and col2a1 mRNA expression as determined by in situ hybridization in relation to the cortical bone. Panel E) The relationship of col1a1 mRNA expression relative to cartilage. Cortical bone is color coded yellow, cartilage red, areas of col1a1 expression blue and col2a1 black. The line of the fracture is depicted by ▪, * denotes the hole from the intramedullary pin.

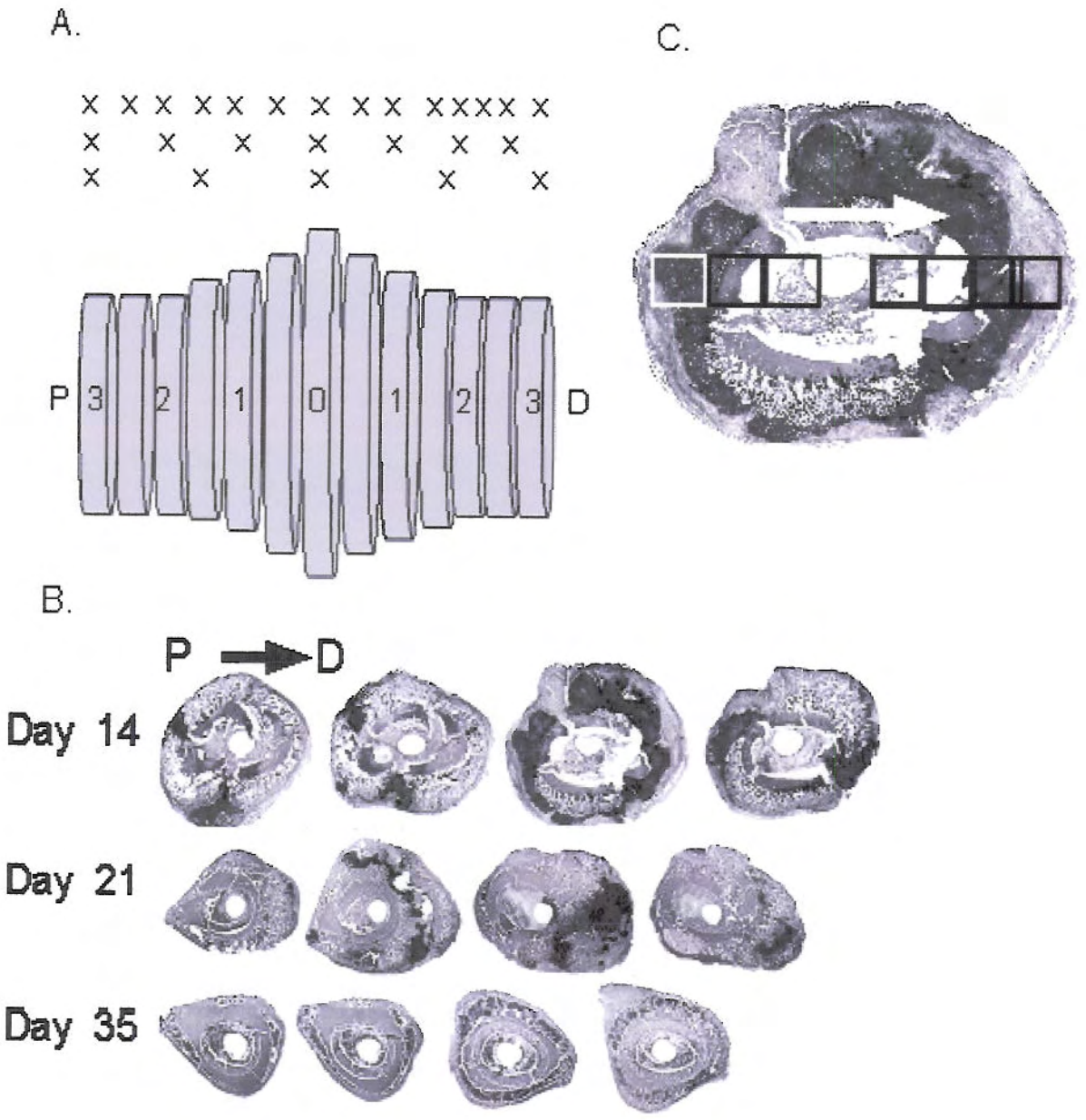

Figure 1

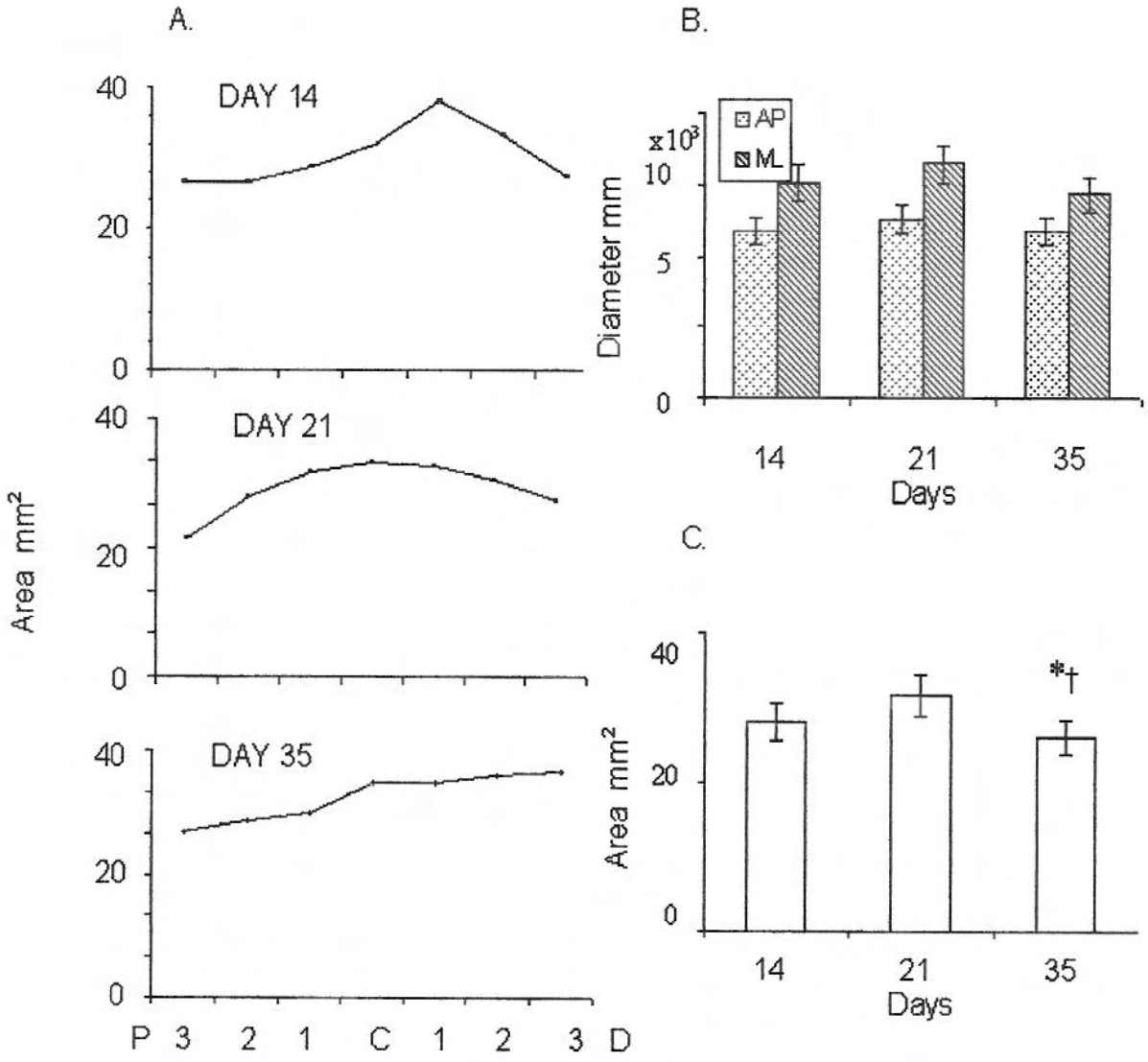
A.
DAY 14
DAY 21
DAY 35
40
20
0
Area mm²
P 3 2 1 C 1 2 3 D
B.
AP
ML
x10³
10
5
0
Diameter mm
14
21
35
Days
C.
40
20
0
Area mm²
*†
14
21
35
Days

Figure 2

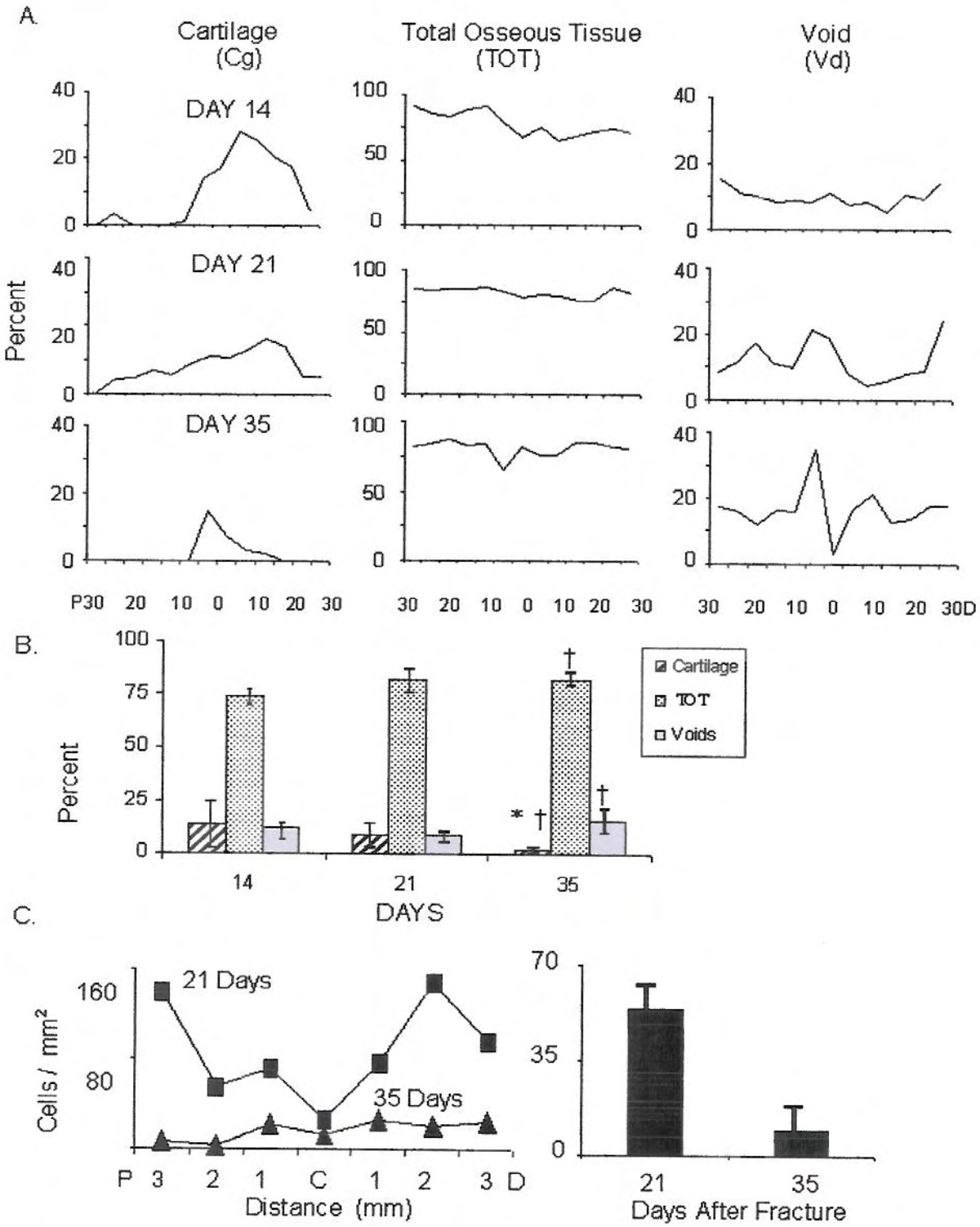
A.
Cartilage (Cg)
Total Osseous Tissue (TOT)
Void (Vd)
DAY 14
DAY 21
DAY 35
Percent
P30 20 10 0 10 20 30
30 20 10 0 10 20 30
30 20 10 0 10 20 30D
B.
Percent
Cartilage
TOT
Voids
14
21
35
DAYS
C.
Cells / mm²
21 Days
35 Days
P 3 2 1 C 1 2 3 D
Distance (mm)
Days After Fracture

Figure 3

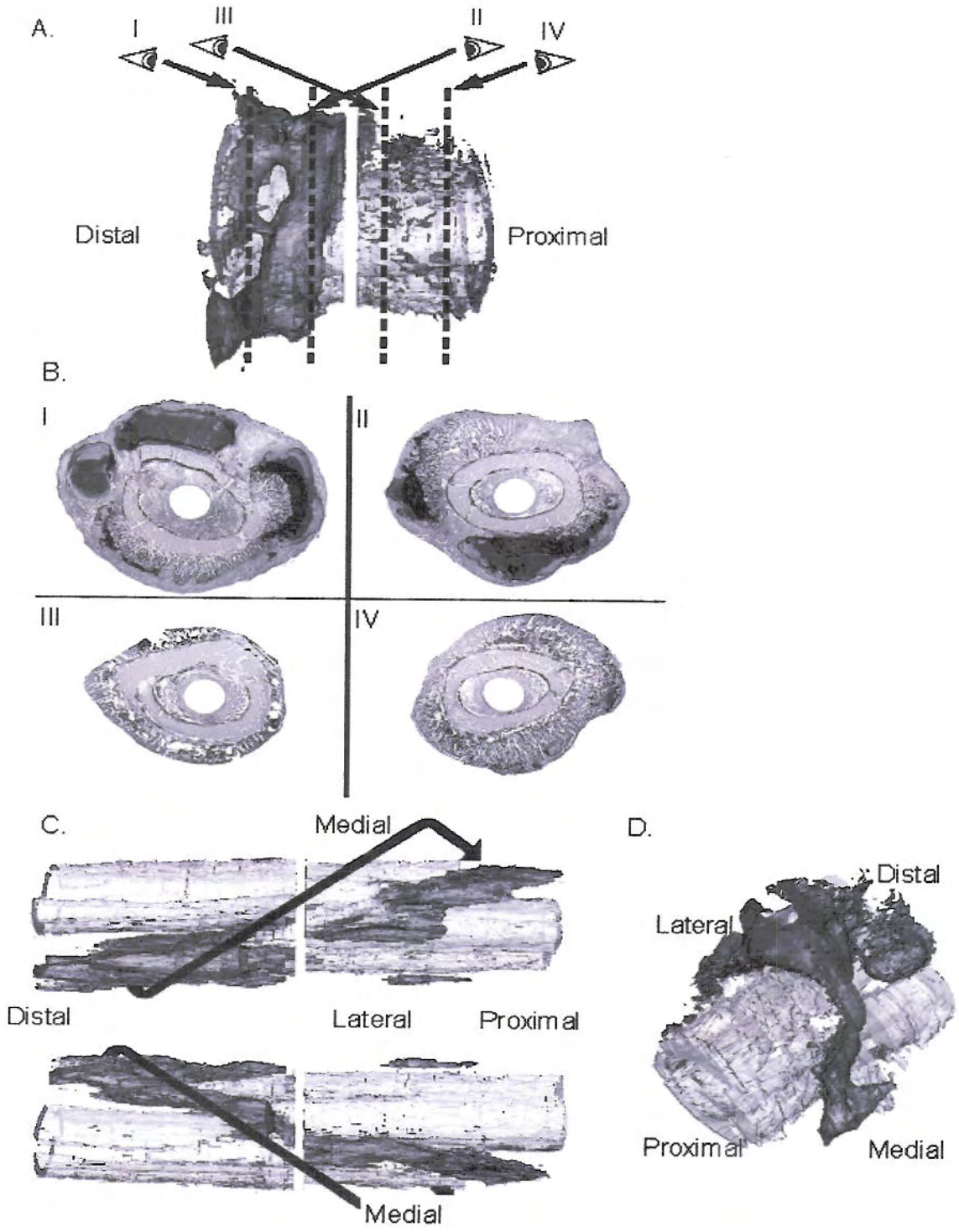
A.
I
III
II
IV
Distal
Proximal
B.
I
II
III
IV
C.
Medial
Distal
Lateral
Proximal
Medial
D.
Distal
Lateral
Proximal
Medial

Figure 4

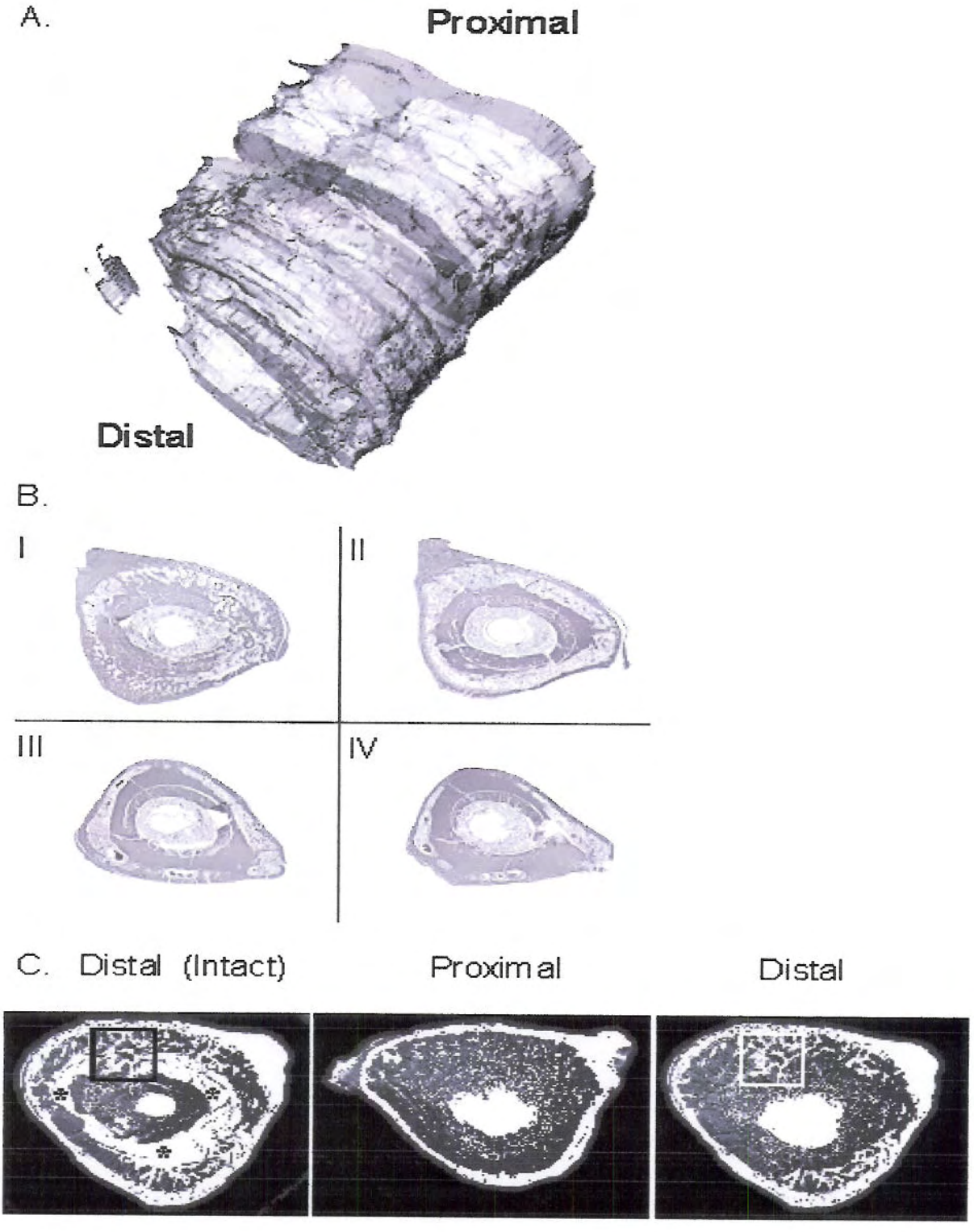
A.
Proximal
Distal
B.
I
II
III
IV
C. Distal (Intact)
Proximal
Distal

Figure 5

Day 7
40X

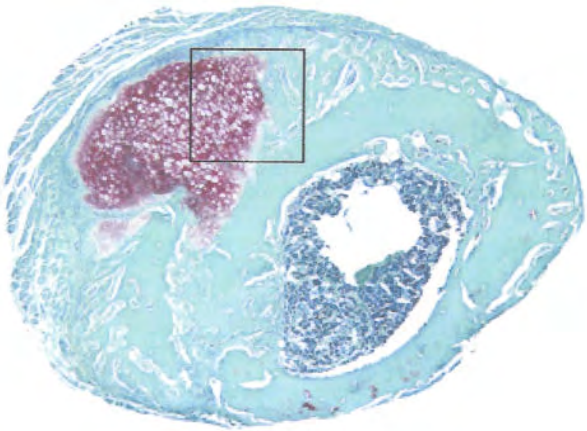

COL1A1

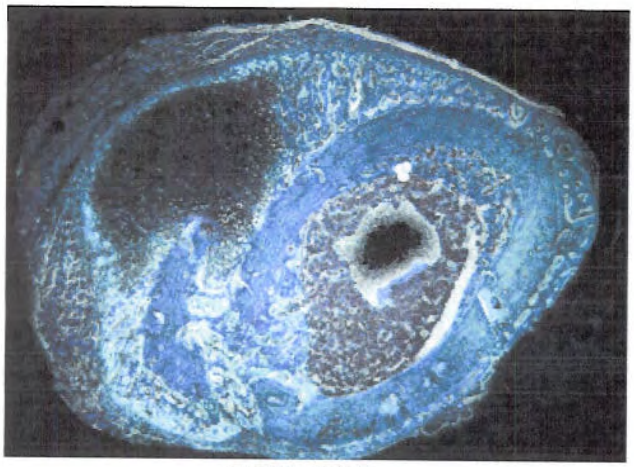

COL2A1

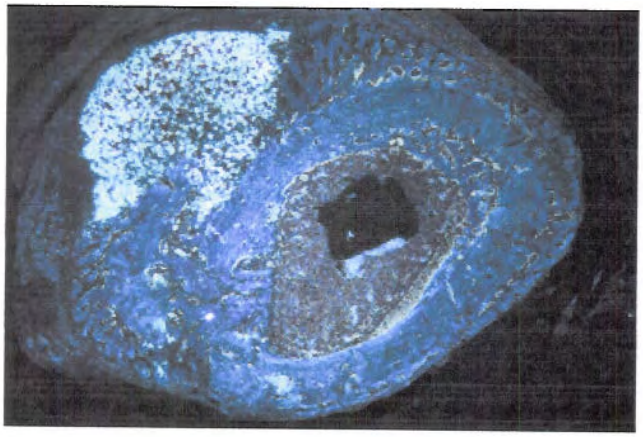

COL1A1
100X

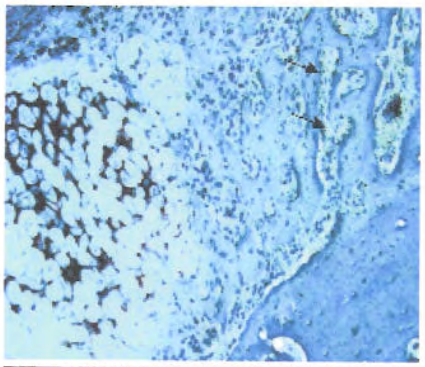

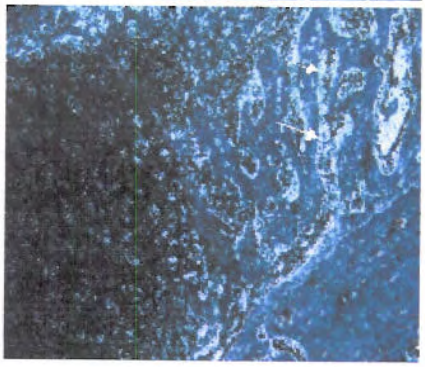

COL2A1

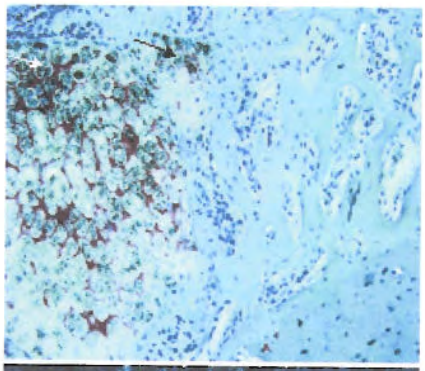

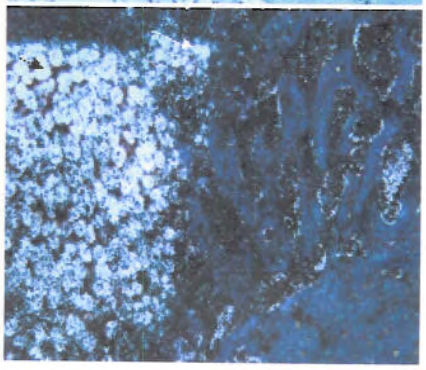

Figure 6

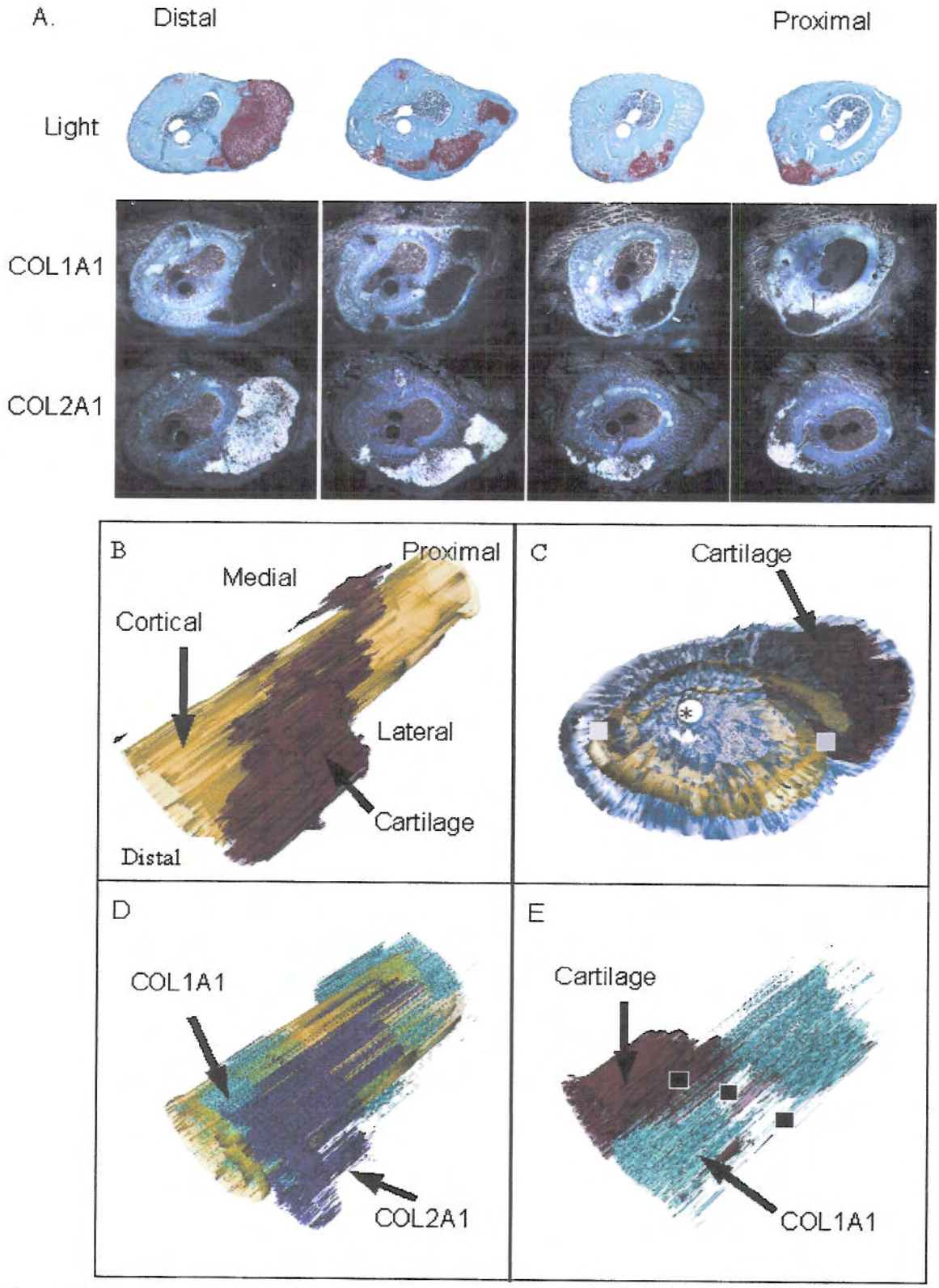
A.
Distal
Proximal
Light
COL1A1
COL2A1
B
Proximal
Medial
Cortical
Lateral
Cartilage
Distal
C
Cartilage
D
COL1A1
COL2A1
E
Cartilage
COL1A1

Figure 7

Table 1. Comparison of Area Composition Versus Volume Compositions in 21-Day Rat Fracture Calluses

Sample	Cartilage	Callus	Cortical Bone	Space
1	16.819	169.084	35.154	10.712
2	20.249	183.589	27.109	18.613
3	10.832	158.645	20.735	10.868
Mean	15.967	170.439	27.666	13.398
Standard Deviation	4.766	12.527	7.226	4.517
Percentage+	9		16 (83*)	8
Percentage # Histomorphometry	9.0		82	9.0

+ Rounded to the nearest whole number

* Total percentage Cortical bone plus all other Non Cartilage Osseous Tissues

Histomorphometry measurements taken from mean values of serial sections taken at every 500□m over the same proximal to distal dimensions as that which was reconstructed. Histomorphometry measurements and tissue volumes were obtained by separate methods of digital image entry.